Dynamical localization in the microwave interaction of Rydberg atoms: The influence of noise

R. Blümel*
Department of Chemistry, University of Pennsylvania, Philadelphia, Pennsylvania 19104-6323

A. Buchleitner†
Sektion Physik der Universität München, D-8046 Garching, Germany
and Max-Planck-Institut für Quantenoptik, D-8046 Garching, Germany

R. Graham
Fachbereich Physik, Universität GHS Essen, D-4300 Essen, Germany

L. Sirko‡
Sektion Physik der Universität München, D-8046 Garching, Germany
and Max-Planck-Institut für Quantenoptik, D-8046 Garching, Germany

U. Smilansky§
H. H. Wills Physics Laboratory, Bristol BS8 1TL, England

H. Walther
Sektion Physik der Universität München, D-8046 Garching, Germany
and Max-Planck-Institut für Quantenoptik, D-8046 Garching, Germany
(Received 26 December 1990; revised manuscript received 13 June 1991)

We present experimental and theoretical results on highly excited Rydberg atoms passing through a waveguide. The waveguide is excited in a coherent mode with a superimposed component of technically generated noise. In the theoretical part of the paper we derive and solve a master equation for a Rydberg atom driven by a monochromatic coherent microwave field in the presence of noise. We show that a Rydberg atom subjected to a mixture of coherent modes and noise fields exhibits four dynamical regimes: (i) diffusive broadening, (ii) localization, (iii) destruction of coherence and localization, and (iv) relaxation to equilibrium. The four regimes are passed one after the other as a function of irradiation time. They occur on different time scales and are thus temporally well separated from each other. The theory is checked by an experiment on the time dependence of the population distribution of highly excited rubidium Rydberg atoms initially prepared in a unique and well-defined Rydberg state and irradiated by a strong microwave field. The localization regime, characterized by a "freezing" of the width of the wave packet with respect to the Rydberg levels, has been observed. The addition of a small noise component was shown to lead to delocalization after times inversely proportional to the noise power, as predicted by our theory.

PACS number(s): 32.80.Rm, 05.45.+b, 05.30.−d

I. INTRODUCTION

Rydberg atoms in strong external microwave fields are interesting candidates for the investigation of nonlinear dynamics [1]: the classical counterpart of this system shows chaos, and it is of special interest to focus attention on the quantum behavior, especially in parameter regions where the classical treatment leads to chaos. One typical phenomenon is the dynamical localization of the population distribution which was discussed in several papers, e.g., by Casati *et al.* [2] and Blümel and Smilansky [3,4], generalizing the concept of localization of the quantum kicked rotor, first noticed by Chirikov, Izraelev, and Shepelyansky [5].

In this paper we investigate the localization and its stability when noise is added to the microwave field. We are concerned here with an important theme of contemporary research, namely the interplay between quantum coherence and external noise. The destruction of quantum coherence by noise is central to many fields of physics and is reflected in the large number of papers recently published on this subject (see, e.g., Refs. [6–20]). Of special interest here is the work reported in Ref. [13] on the influence of controlled noise on the Hanle effect.

Contrary to other experiments, we do not focus on the microwave ionization probability, but on atoms which were not ionized in the microwave region. This is a considerable advantage, especially for the observation of the population redistribution in the external microwave fields (see also Ref. [19] for comparison).

The excitation and ionization behavior of a given Rydberg state under the influence of an external strong microwave field is essentially controlled by three parameters: the microwave field strength, the microwave fre-

quency, and the interaction time. While in existing experiments on the microwave ionization of hydrogen Rydberg atoms [19–23] at least one of the three parameters is hard to change (e.g., the interaction time), our experimental setup is "universal" in the sense that all three control parameters can easily be varied. Out of the three parameters, the variable interaction time is of particular interest. A variable interaction time, e.g., is necessary to clarify whether the phenomenon of quantum localization is present which manifests itself by a stationary population distribution of Rydberg levels around the originally excited level. If the atomic wave function is localized, a change of the interaction time with the microwave field should not change the population distribution.

Recently it was pointed out by Breuer, Dietz, and Holthaus [24] and Breuer and Holthaus [25], that there can be a crucial contribution of the switching on and switching off of the microwave field to the atomic dynamics. Adiabatic switching is indeed important for our experiment and we will come back to this point later (see Sec. IV).

Localization may occur for weak coupling as a perturbative effect [26], or, for strong coupling, it may be interpreted as a form of Anderson localization [27]. In both cases it crucially depends on the coherence of the wave function. The weak-coupling and the strong-coupling regimes are usually identified with respect to the corresponding classical system. In the weak-coupling case population is neither transferred classically nor quantum mechanically. The atomic system is therefore called trivially or perturbatively localized [26]. In the strong-coupling case, the classical system generically shows unlimited diffusion in phase space while in the corresponding quantum system the diffusion may stop after a certain characteristic break time t^* [2,5]. For times $t > t^*$, the quantum system will show the "collapse" and "revival" phenomenon well known in quantum systems with a finite number of levels. This indicates that in the quantum case and due to interference effects, the atomic population is dynamically restricted to a finite set of levels, although, and judging from the behavior of the corresponding classical system, many more levels are in fact strongly coupled and should be accessible for a redistribution of population. Thus, the quantum-mechanical freezing of the atomic population for $t > t^*$ cannot be understood in a classical picture. The quantum freezing effect is therefore called nontrivial localization [2,5,27]. Indeed, one of the main results of this paper will be the experimental demonstration of nontrivial localization in the case of microwave-driven rubidium atoms. While in the theoretical part of the paper classical calculations are readily available to establish the presence of nontrivial localization (see Sec. II), classical calculations for microwave-driven rubidium atoms are understandably not yet available. Nevertheless, we will present convincing arguments to establish the nontrivial nature of the observed localization of rubidium Rydberg states (see Sec. III).

In the case of the kicked rotor, the presence of a small stochastic contribution to the kicking force of the rotor was shown to be sufficient to destroy localization and to lead back to diffusion on long time scales [8,11]. Recently the effects of dissipation and fluctuations, related by the fluctuation-dissipation relation on the localization of the angular momentum of the kicked rotor, has been investigated [9,28]. The dissipation was modeled by a reservoir coupling, resulting in a master equation for the statistical operator of the rotor. Its solution showed that the coherence of the initial state and the accompanying localization are destroyed on a time scale inversely proportional to the dissipation rate or noise intensity. For longer times it was found that the system returns to diffusion, caused by transitions between quasienergy states due to the reservoir coupling.

In the present paper we study theoretically and experimentally the relevance of these results to Rydberg atoms in strong microwave fields, applying similar methods.

The paper is organized as follows: in Sec. II we present the theory and in Sec. III we give the experimental results. In Sec. IV we discuss theoretical and experimental results and Sec. V concludes the paper.

II. THEORY

The theory consists of three parts. In Sec. II A we present a derivation of the master equation of a strongly driven Rydberg atom in the presence of a noise field. Since the atoms are driven strongly by an external microwave field, our master equation is based on the atomic Floquet states rather than on the unperturbed atomic states. Limiting cases of the master equation are studied in Sec. II B. The master equation is solved in Sec. II C in the case of a one-dimensional model. The field parameters are chosen such that the theoretical calculations are of relevance for the experiments described in Sec. III.

A. Derivation of the master equation

In this section we set up the master equation describing the dynamics of Rydberg atoms interacting with strong microwave fields and with thermal fields or externally imposed noise fields. The latter case can be considered as a special case of the former and will be treated at the end of this section. We shall use the Markovian approximation. While the general method of derivation of Markovian master equations is described, e.g., in Refs. [29] and [30], our approach, based on the atomic Floquet states and emphasizing localization properties is sufficiently novel to justify the following detailed presentation of its derivation.

1. Hamiltonian

Consider Rydberg atoms transversely passing a rectangular waveguide held at temperature T and coherently excited in its TE_{01} mode. Figure 1 shows the geometry of the waveguide together with the electric-field distribution of the TE_{01} mode and the direction and position of the coordinate axes. The extension of the waveguide in x and y direction is ξ and η, respectively. The atoms enter the waveguide through the hole at ($x=0$, $y=\eta/2$, $z=0$) and leave the waveguide through the hole at ($x=\xi$, $y=\eta/2$, $z=0$). This way the atoms encounter a constant electric field during most of their passage through the waveguide.

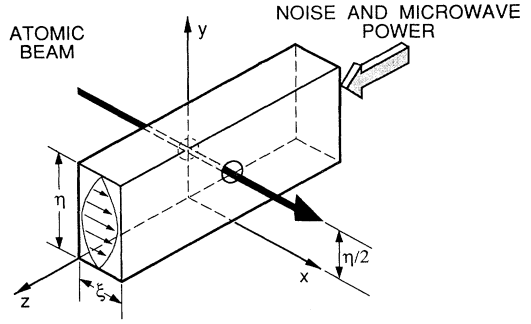

FIG. 1. Sketch of the waveguide used to study Rydberg atoms in a superposition of a strong microwave driving field and a thermal or technically generated noise field.

This setup has to be contrasted with the setup used, for instance, in the Bayfield waveguide experiments, [19,20] where the atoms enter in the y direction and thus encounter an electric field that changes spatially with a sine envelope.

Before the atoms enter the waveguide in the x direction, i.e., parallel to the electric vector of the microwave field, they are prepared in a Rydberg state, i.e., in a highly excited eigenstate of the atomic Hamiltonian $H_{\rm at}$. The total Hamiltonian takes the form

$$H(t)=H_0(t)+H_{\rm int}+H_R \tag{1}$$

with

$$\begin{aligned} H_0(t)&=H_{\rm at}+exF\sin(\omega t)\ , \\ H_{\rm int}&=\hbar\sum_i x(g_i b_i+g_i^* b_i^\dagger)\ , \\ H_R&=\hbar\sum_i \omega_i(b_i^\dagger b_i+\tfrac{1}{2})\ . \end{aligned} \tag{2}$$

H_0 is the Hamiltonian of the Rydberg atom with a dipole coupling to the electric field of the microwave with amplitude F and frequency ω. We assume, for simplicity, that the atom was prepared in an extremal parabolic substate such that only the x component of the dipole moment effectively couples to the electric field. The dipole coupling of the atom to the quantized modes of the waveguide is described by $H_{\rm int}$. The coupling constants g_i are determined below. In the limit of infinite length of the waveguide the sum over i is replaced by

$$\sum_i \rightarrow \sum_{m,n,\lambda}\int d\omega\,\rho_{mn}^{(\lambda)}(\omega)\ , \tag{3}$$

where $\rho_{mn}^{(\lambda)}(\omega)$ is the density of TM_{mn} modes ($\lambda=1$) or TE_{mn} modes ($\lambda=2$) of the waveguide, which is also determined below. Finally, the Hamiltonian of the free field in the waveguide is described by the Hamiltonian H_R. The operators $b_i^\dagger, b_i$ are the usual Bose creation and annihilation operators. In the case of externally imposed classical noise fields the free-field Hamiltonian H_R is to be omitted and the $b_i^\dagger, b_i$ are treated as classical complex mode amplitudes whose averaged absolute square determines the average noise energy at frequency ω_i in units of $\hbar\omega_i$.

2. *Coupling to the quantized modes of the waveguide*

In order to determine the functions g_i and $\rho_{mn}^{(\lambda)}(\omega)$ we have to consider the field quantization (see, e.g., Ref. [31]) in the waveguide. The vector potential in the Heisenberg picture

$$\mathbf{A}(x,y,z,t)=\mathbf{A}^{(-)}(x,y,z,t)+\mathbf{A}^{(+)}(x,y,z,t) \tag{4}$$

in the radiation gauge may be expanded as

$$\begin{aligned} \mathbf{A}^{(+)}(\mathbf{r},t)&=\sum_{l,m,n}\sum_{\lambda}\left[\frac{2\pi c^2\hbar}{\omega_{lmn}}\right]^{1/2} b_{lmn}^{(\lambda)}e^{-i\omega_{lmn}t}\mathbf{U}_{lmn}^{(\lambda)}(\mathbf{r})\ , \\ \mathbf{A}^{(-)}&=(\mathbf{A}^{(+)})^\dagger\ , \end{aligned} \tag{5}$$

where the index λ distinguishes TM ($\lambda=1$) and TE ($\lambda=2$) modes and $\omega_{lmn}=\omega$ is the dispersion relation of the waveguide. The mode functions $\mathbf{U}_{lmn}^{(\lambda)}$ are assumed to be normalized

$$\int_V d\mathbf{r}[\mathbf{U}_{lmn}^{(\lambda)}(\mathbf{r})]^*\cdot\mathbf{U}_{l'm'n'}^{(\lambda')}(\mathbf{r})=\delta_{ll'}\delta_{mm'}\delta_{nn'}\delta_{\lambda\lambda'}\ , \tag{6}$$

where the integration is extended over the volume V of the waveguide. The mode indices l,m,n appear due to the boundary conditions of the waveguide. In the z direction (index l), we assume cyclic boundary conditions over a length L, with $L\rightarrow\infty$ eventually being taken. The boundary conditions in the x and y direction yield the labels m and n, respectively. The Hamiltonian $H_{\rm int}$ now takes the form

$$H_{\rm int}=-\frac{ex}{c}[\dot{A}_x^{(+)}(\mathbf{r},t)+\dot{A}_x^{(-)}(\mathbf{r},t)]_{\mathbf{r}=\mathbf{r}_0(t)}\ , \tag{7}$$

where $\mathbf{r}_0(t)$ is the time-dependent position of the atom in the waveguide. According to our assumptions (see Fig. 1) only the x coordinate of the atom changes with time. Its y and z coordinates are time independent and given by $y=\eta/2$ and $z=0$. Inserting (5) in (7) and comparing with (2) we find the coupling constant

$$g_{lmn}^{(\lambda)}=i\left[\frac{2\pi e^2\omega_{lmn}}{\hbar}\right]^{1/2}\mathbf{e}_x\cdot\mathbf{U}_{lmn}^{(\lambda)}\left[x(t),\frac{\eta}{2},0\right]\ . \tag{8}$$

We now average over the time dependence introduced by $x(t)$. As the final expressions will only depend on $|g_{lmn}^{(\lambda)}|^2$ we take the average in this latter expression, i.e., we make the replacement

$$\left|\mathbf{e}_x\cdot\mathbf{U}_{lmn}^{(\lambda)}\left[x(t),\frac{\eta}{2},0\right]\right|^2 \rightarrow\frac{1}{\xi}\int_0^\xi dx\left|\mathbf{e}_x\cdot\mathbf{U}_{lmn}^{(\lambda)}\left[x,\frac{\eta}{2},0\right]\right|^2\ . \tag{9}$$

The normalized mode functions are for $\lambda=1$

$$\frac{\mathbf{U}_{lmn}^{(1)}}{\mathcal{N}_{lmn}^{(1)}}=\begin{pmatrix} \cos\dfrac{m\pi x}{\xi}\sin\dfrac{n\pi y}{\eta} \\ \dfrac{n\xi}{m\eta}\sin\dfrac{m\pi x}{\xi}\cos\dfrac{n\pi y}{\eta} \\ \dfrac{-i\omega_{mn}^2}{c^2k_l}\dfrac{\xi}{m\pi}\sin\dfrac{m\pi x}{\xi}\sin\dfrac{n\pi y}{\eta} \end{pmatrix}e^{ik_l z} \tag{10}$$

with

$$k_l = 2\pi l / L \ ,$$

$$\omega_{mn} \equiv \omega_{0mn} = \pi c \left[\left[\frac{m}{\xi} \right]^2 + \left[\frac{n}{\eta} \right]^2 \right]^{1/2} ,$$

and

$$\mathcal{N}^{(1)}_{lmn} = \frac{2}{(\xi^3 \eta L)^{1/2}} \frac{m \pi c^2 k_l}{\omega_{lmn} \omega_{mn}} \ , \tag{11}$$

where $m \geq 1$, $n \geq 1$.

For $\lambda = 2$

$$\frac{\mathbf{U}^{(2)}_{lmn}}{\mathcal{N}^{(2)}_{lmn}} = \begin{pmatrix} \cos\frac{m\pi x}{\xi} \sin\frac{n\pi y}{\eta} \\ \frac{m\eta}{n\xi} \sin\frac{m\pi x}{\xi} \cos\frac{n\pi y}{\eta} \\ 0 \end{pmatrix} e^{ik_l z} \ , \tag{12}$$

with

$$\mathcal{N}^{(2)}_{lmn} = \frac{2}{(\xi \eta^3 L)^{1/2}} \frac{n \pi c}{\omega_{mn}} \ , \tag{13}$$

where $m \geq 0$, $n \geq 0$, but $m = n = 0$ is forbidden. Upon averaging on x, the coupling constant (8) becomes

$$g^{(\lambda)}_{lmn} = \left[\frac{\pi e^2 \omega_{lmn}}{\hbar} \right]^{1/2} \times \begin{cases} \mathcal{N}^{(1)}_{lmn} & \text{for } \lambda = 1,\ n \text{ odd},\ m \geq 1 \\ \mathcal{N}^{(2)}_{lmn} & \text{for } \lambda = 2,\ n \text{ odd},\ m \geq 0 \\ 0 \text{ otherwise} \ . \end{cases} \tag{14}$$

As the atomic dipole moment has only a component in the x direction, only modes with $E_x \neq 0$ are "seen" by the atom and need to be considered in the following. These are all the TM and TE modes, except all modes with even n whose **E** vector points in the y direction and therefore do not couple to the dipole moment in the x direction.

In the following the density of modes $\rho^{(\lambda)}_{mn}(\omega)$ will also be needed. From the dispersion relation

$$|k_l| = \frac{\omega_{lmn}}{c} \left[1 - \frac{\omega^2_{mn}}{\omega^2_{lmn}} \right]^{1/2} \tag{15}$$

and the relation, valid for $L \to \infty$,

$$\sum_l \cdots \to \int dl \cdots \to \int_0^\infty d\omega \, \rho^{(\lambda)}_{mn}(\omega) \cdots \ , \tag{16}$$

we find

$$\rho^{(\lambda)}_{mn}(\omega) = \frac{LD}{2\pi c} \frac{\omega}{(\omega^2 - \omega^2_{mn})^{1/2}} \ . \tag{17}$$

Here, $D = 1$ in case technical noise is fed into the waveguide at one end and propagates unreflected along the waveguide, and $D = 2$ in case of thermal noise, or a waveguide filled with technical noise propagating in both z directions. $D = 1$ is the proper choice for the experiments to be described below, since here the noise is fed in at one end of the waveguide (see Fig. 1) and absorbed by a stopper at the other end (not shown in Fig. 1). The coupling of the atom to the quantized field in the waveguide is now completely specified.

3. *Equations of motion in the interaction picture*

The von Neumann equation for the statistical operator ρ of the total system reads

$$i\hbar\dot{\rho} = [H(t), \rho] \ . \tag{18}$$

Our aim now is to treat the interaction with the strong coherent microwave field exactly, and to apply perturbation theory with respect to the coupling to the other modes of the waveguide, which are excited thermally or by externally imposed noise. Therefore, we introduce an interaction picture via the unitary transformation

$$U(t) = U_0(t) \otimes U_R(t) \ ,$$

$$U_0(t) = \left[\exp\left[-\frac{i}{\hbar} \int_0^t d\tau \, H_0(\tau) \right] \right]_+ \ , \tag{19}$$

$$U_R(t) = \exp\left[-\frac{i}{\hbar} H_R t \right] \ ,$$

where $H_0(t), H_R$ are defined by (1) and $[\cdots]_+$ denotes time ordering. The statistical operator in the interaction representation is

$$\tilde{\rho}(t) = U(t) \rho(t) U(t) \ . \tag{20}$$

Using the equation

$$i\hbar\dot{U}(t) = [H_0(t) + H_R] U(t) \ , \tag{21}$$

we obtain the equation of motion in the interaction picture

$$i\hbar\dot{\tilde{\rho}}(t) = [\tilde{H}_{\text{int}}(t), \tilde{\rho}(t)] \tag{22}$$

with the Hamiltonian in the interaction picture

$$\tilde{H}_{\text{int}}(t) = U^\dagger(t) H_{\text{int}} U(t) \ . \tag{23}$$

In order to explicitly construct the operator $U(t)$ it is necessary to solve the Schrödinger equation generated by the Hamiltonian $H_0(t)$. This task has been performed numerically in previous work [3,4,32] on which we shall rely in the following. Let us assume therefore, that the atomic Floquet states $|\Phi_\alpha(t)\rangle$ and the associated quasienergies $\hbar\mu_\alpha$ satisfying

$$U_0(t) |\Phi_\alpha(0)\rangle = e^{-i\mu_\alpha t} |\Phi_\alpha(t)\rangle \ ,$$

$$\left| \Phi_\alpha \left[t + \frac{2\pi}{\omega} \right] \right\rangle = |\Phi_\alpha(t)\rangle \tag{24}$$

are known. We then have for $U_0(t)$

$$U_0(t) = \sum_\alpha e^{-i\mu_\alpha t} |\Phi_\alpha(t)\rangle \langle \Phi_\alpha(0)| \ . \tag{25}$$

For the operators

$$\tilde{b}_i = U^\dagger(t) b_i U(t) ,$$
$$\tilde{x} = U^\dagger(t) x U(t) , \tag{26}$$

we obtain

$$\tilde{b}_i = b_i e^{-i\omega t}, \quad \tilde{b}_i^\dagger = b_i^\dagger e^{i\omega_i t} ,$$
$$\tilde{x}(t) = \sum_{\alpha,\beta} K_{\alpha\beta}(t) |\Phi_\alpha(0)\rangle\langle\Phi_\beta(0)| , \tag{27}$$

with

$$K_{\alpha\beta}(t) = e^{i(\mu_\alpha - \mu_\beta)t} \langle \Phi_\alpha(t)|x|\Phi_\beta(t)\rangle . \tag{28}$$

Introducing the Fourier expansion

$$\langle \Phi_\alpha(t)|x|\Phi_\beta(t)\rangle = \sum_{k=-\infty}^{+\infty} e^{ik\omega t} X_{\alpha\beta}(k) , \tag{29}$$

we can rewrite (27) as

$$\tilde{x}(t) = \sum_{\alpha\beta k} e^{i\Delta_{\alpha\beta}(k)t} X_{\alpha\beta}(k) |\Phi_\alpha(0)\rangle\langle\Phi_\beta(0)| \tag{30}$$

with

$$\Delta_{\alpha\beta}(k) = \mu_\alpha - \mu_\beta + k\omega . \tag{31}$$

Later we shall use the abbreviation

$$\Omega_{\alpha\beta}(k) = |\Delta_{\alpha\beta}(k)| . \tag{32}$$

We note the useful symmetries

$$K_{\alpha\beta}(t) = K^*_{\beta\alpha}(t) ,$$
$$X_{\alpha\beta}(k) = X^*_{\beta\alpha}(-k) , \tag{33}$$
$$\Delta_{\alpha\beta}(k) = -\Delta_{\beta\alpha}(-k) .$$

We are now in a position to write down the Hamiltonian in the interaction representation. Doing so we shall make the "rotating-wave" approximation, i.e., we shall keep only terms $\sim\exp\{\pm i[\Omega_{\alpha\beta}(k)-\omega_i]t\}$ and neglect terms $\sim\exp\{\pm i[\Omega_{\alpha\beta}(k)+\omega_i]t\}$. Then we obtain

$$\tilde{H}_{\rm int} = \hbar \sum_i g_i \sum_{\alpha,\beta,k} \left[\frac{1+\mathrm{sgn}[\Delta_{\alpha\beta}(k)]}{2} X_{\alpha\beta}(k) e^{i[\Omega_{\alpha\beta}(k)-\omega_i]t} |\Phi_\alpha(0)\rangle\langle\Phi_\beta(0)| b_i + \text{H.c.} \right] , \tag{34}$$

where H.c. denotes the Hermitian conjugate, and $\mathrm{sgn}[\Delta_{\alpha\beta}(k)] = \Delta_{\alpha\beta}(k)/\Omega_{\alpha\beta}(k)$.

4. *Elimination of the heat bath*

Our aim is to derive an equation of motion for the reduced density operator $\tilde{\sigma}(t)$ in the interaction picture defined by the trace over the reservoir states

$$\tilde{\sigma}(t) = \mathrm{Tr}_R \tilde{\rho}(t) . \tag{35}$$

We assume that the interaction with the reservoir is switched on adiabatically at $t \to -\infty$ and that for $t \to -\infty$

$$\tilde{\rho}(-\infty) = \tilde{\sigma}(-\infty) \otimes \rho_R \tag{36}$$

with

$$\rho_R = \exp(-H_R/k_B T)/Z_R . \tag{37}$$

Here, k_B is the Boltzmann constant and Z_R is the partition function of the reservoir. $\tilde{\sigma}(t)$ satisfies the integro-differential equation

$$\dot{\tilde{\sigma}}(t) = \mathrm{Tr}_R \left[\frac{1}{i\hbar} [\tilde{H}_{\rm int}(t), \tilde{\rho}(-\infty)] + \frac{1}{(i\hbar)^2} \int_{-\infty}^{t} d\tau [\tilde{H}_{\rm int}(t), [\tilde{H}_{\rm int}(\tau), \tilde{\rho}(\tau)]] \right] . \tag{38}$$

The first term under the trace vanishes because

$$\mathrm{Tr}_R b_i \rho_R = 0 = \mathrm{Tr}_R b_i^\dagger \rho_R . \tag{39}$$

In the second term we may replace $\tilde{\rho}(\tau)$ up to second order in the coupling constants g_i by its zeroth-order approximant

$$\tilde{\rho}(\tau) \approx \tilde{\sigma}(\tau) \otimes \rho_R . \tag{40}$$

Then the trace over the reservoir brings into play the two correlation functions

$$K_1^{(\pm)}(t-\tau) = \sum_i \langle b_i b_i^\dagger \rangle |g_i|^2 e^{\pm i[\omega_i - \Omega_{\alpha\beta}(k)](t-\tau)} ,$$
$$K_2^{(\pm)}(t-\tau) = \sum_i \langle b_i^\dagger b_i \rangle |g_i|^2 e^{\pm i[\omega_i - \Omega_{\alpha\beta}(k)](t-\tau)} , \tag{41}$$

with

$$\langle b_i^\dagger b_j \rangle = \mathrm{Tr}_R\, b_i^\dagger b_j \rho_R = n_{\mathrm{th}}(\omega_i)\delta_{ij} \ , \tag{42}$$

where $n_{\mathrm{th}}(\omega_i)$ is the number of photons in mode number i. In the case of thermal noise, n_{th} is given by Planck's formula $n_{\mathrm{th}}(\omega_i)=[\exp(\hbar\omega_i/k_B T)-1]^{-1}$.

We shall now assume that the reservoir is Markovian, i.e., the correlation functions (41) decay to zero on a time scale τ_0 much smaller than the typical time scales

$$\tau_{\alpha\beta}(k)=\gamma_{\alpha\beta}(k)^{-1} \tag{43}$$

of the master equation [see (49) below]. Then we may replace for $\tau \geq \tau'$

$$K_1^{(\pm)}(\tau-\tau')=2\pi\delta(\tau-\tau')\sum_{m,n,\lambda}\left[\rho_{mn}^{(\lambda)}(\Omega_{\alpha\beta}(k))|g_{mn}^{(\lambda)}(\Omega_{\alpha\beta}(k))|^2[1+n_{\mathrm{th}}(\Omega_{\alpha\beta}(k))]\right.$$
$$\left.\pm iP\int\frac{d\omega}{\pi}\frac{\rho_{mn}^{(\lambda)}(\omega)|g_{mn}^{(\lambda)}(\omega)|^2[1+n_{\mathrm{th}}(\omega)]}{\omega-\Omega_{\alpha\beta}(k)}\right] , \tag{44}$$

where P indicates a principal-value integral. A corresponding expression for $K_2^{(\pm)}(\tau-\tau')$, where $(1+n_{\mathrm{th}})$ is replaced by n_{th}, is easily derived. We used the mode density introduced in (16) and employed the notation $g_{mn}^{(\lambda)}(\omega)=g_{lmn}^{(\lambda)}$ for $|l|=(\omega L/2\pi c)(1-\omega_{mn}^2/\omega^2)^{1/2}$.

In the following we shall neglect the principal part in expression (44) which describes a shift of the quasienergies induced by the reservoir. The integro-differential equation now reduces to a differential equation which takes the form

$$\dot{\tilde{\sigma}}(t)=\pi\sum_{\alpha,\beta,k}\sum_{\alpha',\beta',k'}\sum_{m,n,\lambda}\frac{1+\mathrm{sgn}[\Delta_{\alpha\beta}(k)]}{2}\frac{1+\mathrm{sgn}[\Delta_{\alpha'\beta'}(k')]}{2}\rho_{mn}^{(\lambda)}(\Omega_{\alpha'\beta'}(k'))|g_{mn}^{(\lambda)}(\Omega_{\alpha'\beta'}(k'))|^2$$
$$\times[X_{\alpha\beta}(k)X_{\alpha'\beta'}^*(k')e^{i[\Omega_{\alpha\beta}(k)-\Omega_{\alpha'\beta'}(k')]t}$$
$$\times\{[1+n_{\mathrm{th}}(\Omega_{\alpha'\beta'}(k'))][\Gamma_{\alpha'\beta'}^\dagger\tilde{\sigma}(t),\Gamma_{\alpha\beta}]+n_{\mathrm{th}}(\Omega_{\alpha'\beta'}(k'))[\Gamma_{\alpha\beta},\tilde{\sigma}(t)\Gamma_{\alpha'\beta'}^\dagger]\}+\mathrm{H.c.}] \ , \tag{45}$$

where we used the notation

$$\Gamma_{\alpha\beta}=|\Phi_\alpha(0)\rangle\langle\Phi_\beta(0)| \ . \tag{46}$$

We now assume that

$$|\Omega_{\alpha\beta}(k)-\Omega_{\alpha'\beta'}(k')|t\gg 1 \tag{47}$$

for all triplets $(\alpha,\beta,k)\neq(\alpha',\beta',k')$, in which case only terms with $(\alpha,\beta,k)=(\alpha',\beta',k')$ must be kept in (45). The master equation in the interaction picture then finally reads

$$\dot{\tilde{\sigma}}(t)=\tfrac{1}{2}\sum_{\alpha\beta k}\gamma_{\alpha\beta}(k)[[1+n_{\mathrm{th}}(\Omega_{\alpha\beta}(k))]\{[\Gamma_{\alpha\beta}^\dagger,\tilde{\sigma}(t)\Gamma_{\alpha\beta}]+[\Gamma_{\alpha\beta}^\dagger\tilde{\sigma}(t),\Gamma_{\alpha\beta}]\}$$
$$+n_{\mathrm{th}}(\Omega_{\alpha\beta}(k))\{[\Gamma_{\alpha\beta},\tilde{\sigma}(t)\Gamma_{\alpha\beta}^\dagger]+[\Gamma_{\alpha\beta}\tilde{\sigma}(t),\Gamma_{\alpha\beta}^\dagger]\}] \tag{48}$$

with

$$\gamma_{\alpha\beta}(k)=2\pi\sum_{m,n,\lambda}\rho_{mn}^{(\lambda)}(\Omega_{\alpha\beta}(k))|g_{mn}^{(\lambda)}(\Omega_{\alpha\beta}(k))|^2$$
$$\times|X_{\alpha\beta}(k)|^2\frac{1+\mathrm{sgn}[\Delta_{\alpha\beta}(k)]}{2} \ . \tag{49}$$

It is convenient to use the representation provided by the basis $|\Phi_\alpha(0)\rangle$ and to write

$$\tilde{\sigma}_{\alpha\beta}(t)=\langle\Phi_\alpha(0)|\tilde{\sigma}(t)|\Phi_\beta(0)\rangle \ . \tag{50}$$

Then the master equation becomes [33,34]

$$\dot{\tilde{\sigma}}_{\alpha\alpha}(t)=\sum_\mu(M_{\mu\alpha}\tilde{\sigma}_{\mu\mu}-M_{\alpha\mu}\tilde{\sigma}_{\alpha\alpha}) \ ,$$
$$\dot{\tilde{\sigma}}_{\alpha\beta}=-\tfrac{1}{2}\left[\sum_\mu(M_{\alpha\mu}+M_{\beta\mu})\right]\tilde{\sigma}_{\alpha\beta}(t)\quad(\alpha\neq\beta) \ , \tag{51}$$

with

$$M_{\alpha\beta}=\sum_{k=-\infty}^{k=\infty}\{\gamma_{\alpha\beta}(k)+n_{\mathrm{th}}(\Omega_{\alpha\beta}(k))$$
$$\times[\gamma_{\alpha\beta}(k)+\gamma_{\beta\alpha}(k)]\} \ . \tag{52}$$

Its solution for the off-diagonal elements is

$$\tilde{\sigma}_{\alpha\beta}(t)=\sigma_{\alpha\beta}(0)\exp\left[-\frac{t}{2}\sum_\mu(M_{\alpha\mu}+M_{\beta\mu})\right]\quad(\alpha\neq\beta) \ . \tag{53}$$

In the Schrödinger picture we then obtain

$$\sigma_{\alpha\beta}(t)=e^{-i(\mu_\alpha-\mu_\beta)t}\tilde{\sigma}_{\alpha\beta}(t) \ . \tag{54}$$

The solution for the diagonal elements is

$$\tilde{\sigma}_{\alpha\alpha}(t)=\sum_{\beta}[\exp(-\Lambda t)]_{\alpha\beta}\tilde{\sigma}_{\beta\beta}(0)\ , \tag{55}$$

where the matrix Λ has the elements

$$\Lambda_{\alpha\beta}=-M_{\beta\alpha}+\delta_{\alpha\beta}\sum_{\mu}M_{\alpha\mu}\ . \tag{56}$$

B. Limiting cases of the master equation

Let us consider as limiting cases the case of no externally applied microwave field (Sec. II B 1) and the case where the reservoir is replaced by externally imposed classical noise (Sec. II B 2).

1. No externally applied microwave field

In this case the Floquet states $|\Phi_\alpha\rangle$ are time independent and given by the eigenstates of the atomic Hamiltonian. The μ_α become the energies of the unperturbed atomic levels. The matrix elements reduce to $X_{\alpha\beta}(k)=X_{\alpha\beta}\delta_{k,0}$ and therefore also $\gamma_{\alpha\beta}(k)=\gamma_{\alpha\beta}\delta_{k,0}$. The master equation (51) retains its form, but the sum over k in (52) reduces to the single term with $k=0$.

The physical effect of the external microwave field on the interaction of the atom with the reservoir can now be appreciated: Without the external microwave field only the reservoir modes in resonance with the atomic transitions effectively interact with the atom [10]. With the external microwave field switched on, reservoir modes at the atomic transition frequencies plus or minus integer multiples of the microwave frequency can also interact with the atom, but the total transition strength

$$\sum_{\beta}\sum_{k}|X_{\alpha\beta}(k)|^2=\frac{\omega}{2\pi}\int_0^{2\pi/\omega}dt\,\langle\Phi_\alpha(t)|x^2|\Phi_\alpha(t)\rangle \tag{57}$$

remains about the same. Whether the presence of the microwave field will tend to stabilize [35] the states $|\Phi_\alpha(t)\rangle$ compared with the energy eigenstates $|\Phi_\alpha\rangle$ therefore depends on the frequency dependence of the reservoir response function

$$\sum_{m,n,\lambda}\rho_{mn}^{(\lambda)}(\omega)|g_{mn}^{(\lambda)}(\omega)|^2[1+n_{\rm th}(\omega)]\ .$$

2. Externally imposed classical noise

In this case the spontaneous decay of a Floquet state of the driven atom by interaction with the reservoir is negligible compared to induced decay and we may put $1+n_{\rm th}\approx n_{\rm th}\gg 1$. Also the distribution of the noise energy over the spectrum need no longer be given by Planck's formula.

Let the number of "noise-quanta" in the mode m,n,λ at frequency ω be $n_{mn}^{(\lambda)}(\omega)$. It can be determined if the noise power $R_{mn}^{(\lambda)}(\omega)d\omega$ in all the TM_{mn} modes ($\lambda=1$) and TE_{mn} modes ($\lambda=2$) at frequency ω in $d\omega$ is specified. We have by standard electrodynamics

$$R_{mn}^{(\lambda)}(\omega)d\omega=\frac{\hbar\omega n_{mn}^{(\lambda)}(\omega)\rho_{mn}^{(\lambda)}(\omega)d\omega}{\xi\eta L}v_{mn}(\xi\eta)\xi\eta\ , \tag{58}$$

where on the right-hand side the first factor specifies the spatial energy density in the mode (m,n) in the frequency interval $d\omega$, the second factor gives the group velocity

$$v_{mn}=c(1-\omega_{mn}^2/\omega^2)^{1/2} \tag{59}$$

with which it propagates down the waveguide, and the third factor gives the cross section of the wave guide. Inserting the spectral density of modes from (17) and solving for $n_{mn}^{(\lambda)}(\omega)$, we obtain

$$n_{mn}^{(\lambda)}(\omega)=\frac{2\pi}{\hbar\omega D}R_{mn}^{(\lambda)}(\omega)\ . \tag{60}$$

Therefore, in the case of externally imposed classical noise, (48) remains valid if in (48) and (49) we replace

$$\begin{aligned}&[1+n_{\rm th}(\Omega_{\alpha\beta}(k))]\rho_{mn}^{(\lambda)}(\Omega_{\alpha\beta}(k))\\ &\quad\approx n_{\rm th}(\Omega_{\alpha\beta}(k))\rho_{mn}^{(\lambda)}(\Omega_{\alpha\beta}(k))\\ &\quad\rightarrow\frac{2\pi}{\hbar\Omega_{\alpha\beta}(k)D}R_{mn}^{(\lambda)}(\Omega_{\alpha\beta}(k))\rho_{mn}^{(\lambda)}(\Omega_{\alpha\beta}(k))\ .\end{aligned} \tag{61}$$

C. Solution of the master equation

In this section we solve numerically the master equation (48) in its matrix representations (53) and (55). In order to compare our theory with the experimental results to be described in Sec. III, the theoretical results for the coherences and populations of quasienergy states, (53) and (55), respectively, have to be transformed back into the atomic basis which yields $\sigma_{nn'}$ and $\sigma_{nn}\equiv P_n$, respectively. On this level, the question arises how to compress the information contained in the set of occupation probabilities $\{P_n\}$ in a physically meaningful way. In the context of information theory, the message conveyed by a particular excited atom in an atomic beam is its state of excitation $|n\rangle$. An atomic beam, therefore, is nothing but a source of information, a transmitter, which generates a sequence of elementary messages ($\equiv$atoms in several possible excited states) which occur with a probability P_n. In other words, it is a stationary stochastic process. In 1948, C. E. Shannon [36] realized that the most fundamental concept which characterizes a transmitter is its entropy $S=-\sum_n P_n\log_2 P_n$, where $\log_2$ is the logarithm with respect to base 2. The entropy S is the minimum average word length required for coding the possible elementary messages $|n\rangle$ in a binary code. This is obvious if the number M of elementary messages is a power of 2, $M=2^m$, and all the elementary messages occur with equal probability $P_n=2^{-m}$. We get $S=-\sum_n P_n\log_2 P_n=m$ which is exactly the number of bits required to code 2^m equiprobable symbols. The Shannon width, $W=2^S=\exp(-\sum_n P_n\ln P_n)$ defines the effective number of distinct elementary messages the transmitter is able to generate. It equals $W=2^m=M$ in our example of 2^m equiprobable elementary messages.

The Shannon width W is a fundamental concept in

analyzing sequences of occupation probabilities $\{P_n\}$ which can, e.g., result from solid-state experiments as occupation probabilities of lattice sites n, or in atomic beam experiments as occupation probabilities of excited states $|n\rangle$. In both cases, the question whether W is finite or infinite is of elementary significance. For $W<\infty$, the set of occupation probabilities $\{P_n\}$ is called localized, whereas $W=\infty$ defines the delocalized situation.

To our knowledge, the concepts of Shannon entropy and width were first used implicitly in an atomic physics context in Refs. [37] and [38] and explicitly in the context of localization in Rydberg atoms in Ref. [3]. The Shannon width is not the only function which measures the spread of population distributions. A wide class of such measures is $\chi_\alpha=\sum_n P_n^\alpha$, $\alpha\geq 1$; $W_\alpha=\chi_\alpha^{-1}$. While for $\alpha=1$ we obtain the trivial result $\chi=1$ which reflects nothing but the normalization of the set $\{P_n\}$; for $\alpha=2$ we obtain $W_2=\chi_2^{-1}=(\sum_n P_n^2)^{-1}$ which is the participation ratio widely used in solid-state physics. We emphasize that different measures of the width of a set $\{P_n\}$ yield generally very different numerical answers. Depending on the specific set $\{P_n\}$ at hand, the Shannon width, the participation ratio, or the more traditional concept of the full width at half maximum (see Sec. III) can differ from each other by substantial numerical factors.

Because of its immediate connection to information theory, we prefer to work with the Shannon width $W=e^S$. Moreover, the Shannon width allows a link to quantum chaos. Since for $W<\infty$, a finite code suffices to identify the outcome of an atomic beam experiment, a stationary probability distribution $\{P_n\}$ with $W<\infty$ (the localized case) cannot show any quantum chaos. A necessary condition for chaos to occur in the sequence of stationary state probabilities P_n is an infinite code, $W=\infty$, which corresponds to the delocalized situation.

With this background in mind, the Shannon width will be the primary subject of investigation in the theoretical as well as in the experimental sections to follow.

1. Method

The master equation (48) was solved numerically for an ideal rectangular waveguide with $\xi=0.953$ cm and $\eta=1.905$ cm. These are exactly the dimensions of the wave guide used in the experiment to be discussed later. We used two temperatures, $T=4$ and 300 K, respectively. Apart from the thermal noise, the waveguide was excited coherently in the TE_{01} mode with amplitude $F=1.56\times10^{-9}$ a.u. and frequency $\omega=1.61\times10^{-6}$ a.u. The atomic Hamiltonian was chosen to describe a one-dimensional model of a hydrogen Rydberg atom [39,40]

$$H_{\rm at}=\frac{p^2}{2}-\frac{1}{x}\quad(x>0)\ . \tag{62}$$

The initial state was chosen as the eigenstate of this Hamiltonian with principal quantum number $n_0=71$. A classical calculation with a sudden switch on of the coherent microwave field (no noise present) shows that this case is characterized by strong classical ionization, yet there is no quantum ionization above the 1% level. The quantum calculations in this case were performed by coupling the continuum as described in Ref. [41]. Twelve atomic bound states $|n\rangle$ ranging from $n=69$ to 80 were used as a basis for the expansion of the Floquet states, which were determined numerically. In this way, the final results could be expressed in the basis of bound states of the hydrogen model. The Shannon width of the resulting probability distribution is given by

$$W(N,T)=\exp\left[-\sum_n P_n(N,T)\ln P_n(N,T)\right]\ , \tag{63}$$

where T is the temperature of the reservoir and

$$P_n(N,T)=\left\langle n\left|\sigma\left[N\frac{2\pi}{\omega}\right]\right|n\right\rangle \tag{64}$$

is the probability to find the state $|n\rangle$ in the statistical mixture described by the statistical operator σ after the atom has experienced N microwave periods. The Shannon width is a convenient measure for the number of states $|n\rangle$ contained in the mixture σ.

2. Results

In Fig. 2 the Shannon width W obtained from the master equation as described in Sec. II C 1 is plotted versus the logarithm of the number of microwave periods N at 100 discrete times N_j, $j=1,\ldots,100$, for $T=4$ and 300 K. The mesh points N_j were selected according to $N_j=[10^{0.12j}]$ where $[x]$ denotes the integer part of x. Initially only a single state $|n_0=71\rangle$ is occupied and therefore $W(N=0,T)=1$. Figure 2 displays four different regimes in time. In the first regime, W increases within the first microwave cycle from its initial value $W(0,T)=1$ to a value of the width which fluctuates around $W=5$ and is independent of the temperature T. In order to conveniently represent all four regimes on one scale, we indicated this rapid initial rise in Fig. 2 by the straight-line segment at $\ln N\approx 0$. The fast temporal rise of W is due to the fact that for the chosen demonstration example $\omega n^3<1$. In this first regime the exposure time is so small

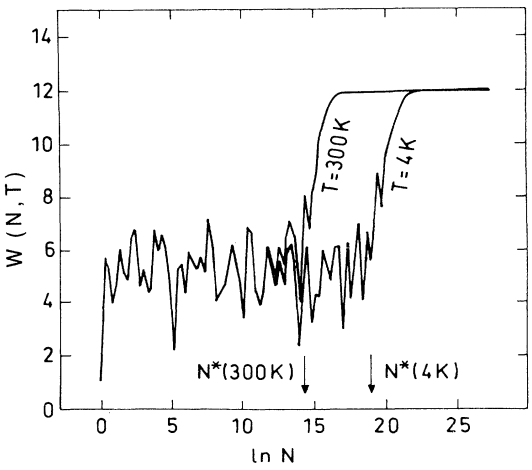

FIG. 2. Width of the $\{P_n\}$ distribution as a function of time for two different temperatures.

that quantum effects due to the discreteness of the quasienergies are not yet relevant. Also the coupling to the reservoir is completely irrelevant in this regime.

In the second regime, W saturates and shows pronounced quasiperiodic oscillations in time (independent of temperature) around an average value significantly larger than 1 but also significantly smaller than the total size of the basis. This is the signature of dynamical localization [27,42]. The large amplitudes of the oscillations show the importance of the coherences $\sigma_{\alpha,\beta}$, $\alpha \neq \beta$ in this regime. The oscillations occur on a time scale of a few microwave cycles. Since only 100 meshpoints were used in Fig. 2 for $N=10^{12}$ microwave cycles, they are not resolved in Fig. 2.

Like in the first regime, the coupling to the reservoir has not yet any noticeable effect in the second (plateau) regime. The second regime is terminated by a transition, which, on the logarithmic time scale of Fig. 2, is sharp, defining the temperature-dependent transition time $N^*(T)$. We have determined this transition time for different temperatures at two different field amplitudes. The result is shown in a doubly logarithmic plot in Fig. 3 for $F=4$ V/cm (circles) and $F=8$ V/cm (squares). The straight line interpolating the data gives the relation $N^*(T)T=\text{const}$. This relation follows from the solution (53) of the master equation in the limit

$$n_{\text{th}}(\Omega_{\alpha\beta}(k)) \approx \frac{k_B T}{\hbar \Omega_{\alpha\beta}(k)} \gg 1 \tag{65}$$

in which case $M_{\alpha\beta} \simeq T$. The limit (65), in fact, applies to our numerical calculations. In the case of technical noise, (61) shows that the number of noise quanta per mode is proportional to the applied noise power R and the relation $N^*(R)R=\text{const}$ should hold where R is the total noise power. In the third dynamical regime, reached for $N > N^*(T)$, the strong fluctuations have essentially ceased and the number of $|n\rangle$-states contained in the mixture increases. The first effect shows that the coherences $\sigma_{\alpha\beta}$, $\alpha \neq \beta$ have decayed after the time $N^*(T)$, the second effect shows that the populations $\sigma_{\alpha\alpha}$ are changed on the same time scale. This is described analytically by (53), (55), and (56). As the rate constants $M_{\alpha\beta}$ are all proportional to T in the simulations, the diagonal elements $\sigma_{\alpha\alpha}$, according to (55), are functions of NT only. If all off-diagonal elements would vanish ($\sigma_{\alpha\beta}=0$), the Shannon width would be determined by the diagonal elements $\sigma_{\alpha\alpha}$ only, and then

$$W(N,T)=\tilde{W}(NT)=\tilde{\tilde{W}}(\ln N+\ln T) . \tag{66}$$

If this scaling relation is satisfied, then in the logarithmic plot of Fig. 2 an increase in T must amount to a parallel shift of the curve to the left. Indeed, it can be seen that in Fig. 2 the parts of the curves for $N > N^*(T)$ approximately satisfy this requirement, which, together with the disappearance of the fluctuations, gives evidence that the coherences have decayed to zero. The fourth and final regime reached for sufficiently long time is a steady state which, in the present case, where $n_{\text{th}}(\Omega_{\alpha\beta}(k)) \gg 1$, corresponds to equidistribution over the whole basis.

These findings for the one-dimensional model of the hydrogen atom correspond closely to results obtained for the mean energy of the kicked rotor model weakly coupled to classical noise [8] or a heat reservoir [28,43,44]. Also there the initial classical diffusive regime is followed by a regime of dynamical localization, where both regimes are independent of the heat reservoir. After a transition time inversely proportional to the noise intensity (or, equivalently, the square of the reservoir coupling constant), the regime of localization goes over into a new diffusive regime, where the diffusion constant is again proportional to the noise intensity.

In summary, we derived and solved a master equation for Rydberg atoms interacting with a strong microwave field in a noisy waveguide. We reached definite theoretical predictions: noise-induced destruction of coherence and localization at a critical interaction time N^*, and redistribution of populations of quasienergy states in a time which scales inversely proportional to temperature or noise intensity.

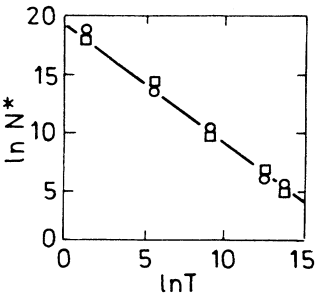

FIG. 3. The relation between temperature and break time N^* for two different field strengths (squares: $F=4$ V/cm; circles: $F=8$ V/cm). The straight line interpolating the data was drawn to guide the eye, and reflects the relation $N^*T=\text{const}$.

III. EXPERIMENT

In this section we present the experiment which is used to check the theoretical predictions. In Sec. III A we describe in detail the setup of our experimental apparatus and the experimental procedures used to access the bound-state probability distribution of rubidium Rydberg atoms which are subjected to a combination of coherent and noisy fields. In Sec. III B we present the experimental results which are evaluated in Sec. III C by means of a deconvolution procedure.

A. Setup and description of the experimental procedure

In contrast to the experiments of Bayfield and Sokol [19,20], Bayfield *et al.* [23], Galvez *et al.* [21], and Moorman *et al.* [22] who work with fast beams of highly excited H atoms, our setup uses a thermal beam of rubidium atoms which can be laser excited to nP Rydberg states ranging from $n=40$ to $n \approx 135$. The laser radia-

tion was produced by frequency doubling the light of a rhodamine 6G laser. Figure 4 shows our setup; laser excitation, microwave interaction, and analyzing regions are spatially well separated from each other. The rubidium atoms leave the oven as a thermal beam with a modified Maxwellian velocity distribution. For the experiments a well-controlled microwave interaction time is required, in principle achievable by velocity selection of the atoms. We used a much simpler and cleaner way which additionally avoids problems with stray fields: after leaving the oven, a group of atoms is laser excited by a short laser pulse (pulse duration 6 μs). The resulting group of Rydberg atoms then travels into the waveguide. Due to the velocity distribution, the bunch of atoms spreads spatially. If the duration of the laser pulse was chosen short enough, this spread of the atoms is smaller than the dimension of the waveguide. As soon as the packet reaches the center of the waveguide, the atoms are irradiated with an electronically shaped, nearly rectangular microwave pulse (TE_{01} mode) whose duration t can be varied from ca. 10 ns to roughly 20 μs. (The maximal interaction time is determined by the time of flight of the atoms through the waveguide.) The microwave pulse is switched on and off by a pin-diode switch which generates a rise- and switch-off time of about 6 ns corresponding to about 70 periods of the microwave field. The carrier frequency can be varied from 8 to 18 GHz. The microwave pulse induces transitions to different Rydberg states, or ionization, depending on the duration, the carrier frequency, and the field strength of the microwave pulse. The packet of Rb atoms, of which every single atom saw exactly the same microwave pulse, is now traveling towards the field-ionization region. Here the atoms are ionized by an electric-field ramp [45] [1.8 V/(cm μs)] and the ejected electrons are detected by a channeltron multiplier. The exact timing of laser excitation, microwave interaction, and field ionization is controlled by a pulse generator and delay lines such that, independently of their particular velocity, the atoms all interact for the same time not only with the microwave field, as mentioned already, but also with the ionizing field ramp in the analyzing region. The latter is important in order to reach a high state selectivity in the detection process.

In all experiments on microwave excitation the most difficult part is the calibration of the microwave field strength in the interaction region. This might be done, in principle, by carefully monitoring the power flux through the waveguide, assisted by a numerical calculation of the resonator modes. We choose a more direct and reliable procedure which determines the electric-field strength inside the waveguide from direct observation of two-photon Rabi nutation between highly excited P states, e.g., $66P_{3/2} \leftrightarrow 67P_{3/2}$ (frequency: 12.634 85 GHz) [46]. For this purpose, we make use of the unique feature of our setup: the interaction time with the microwave can be varied. The Rabi oscillation occurs due to the modulation of the population in the upper state (e.g., $67P_{3/2}$) as a function of the microwave pulse duration (see Fig. 5, and Ref. [47] for more details). The field strength can now be evaluated from the known matrix elements [48] for the induced microwave transition, and from the Rabi frequency found in the experiment.

B. Experimental results for coherent and noisy microwave drive

For the experimental investigation of the localization properties of highly excited Rydberg atoms [3,4,32,49] we prepared the atoms in the $84P_{3/2}$ state. Electronic shot noise (generated by an idling traveling-wave tube amplifier [19,20] and ranging from 8 to 18 GHz) can be admixed to the coherent microwave pulses (carrier frequency 12.059 44 GHz) in arbitrary ratios. In the field-ionization region, the different Rydberg states are ionized at different times within the field ramp. If $G(E;t)$ is defined as the ionization probability at ramp field E of atoms having interacted a time t with the microwave field to which a noise contribution was added, then this probability will be a unique function of the final bound-state distribution of the Rydberg atoms. In the following we denote by $G^{(c)}(E;t)$ the response function of atoms which have interacted with the coherent microwave alone, and by $G^{(s)}(E;t)$ the response to a superposition of coherent signal with noise. $G^{(n_0)}(E)$ $[\tilde{G}^{(n_0)}(E)]$ shall represent the

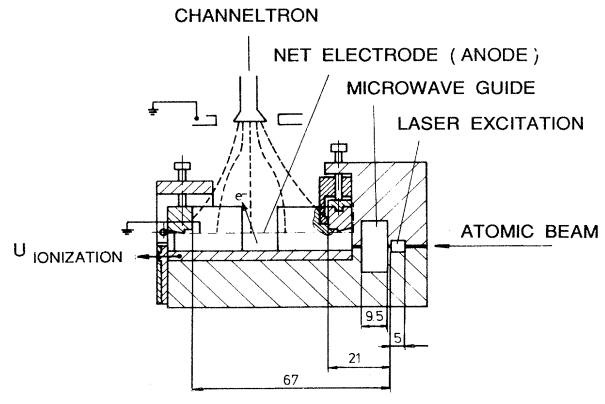

FIG. 4. Side view of the experimental block. Laser excitation, microwave interaction, and analyzing region are spatially well separated from each other. Lengths are indicated in mm.

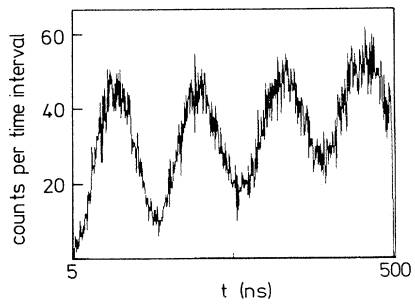

FIG. 5. Two-photon Rabi nutations for the transition $66P_{3/2}$-$67P_{3/2}$. Microwave frequency: 12.634 85 GHz; power: 2.48 μW.

normalized (non-normalized) ionization probability of atoms which neither interacted with the coherent signal nor with noise; this function is therefore the characteristic field-ionization signature of the pure state $n_0P_{3/2}$ initially prepared by laser interaction.

In Figure 6, some typical results for $\tilde{G}^{(n_0)}(E)$ are shown, with n_0 ranging from 68 to 110. The curves represent the directly recorded signals without normalization. Since the slew rate of the ionization-field ramp has been kept constant for all the measurements we are reporting here, these pictures show the dependence of the field-ionization signals on the principal quantum number [50–52]. The rather complicated structure of these curves is a consequence of diabatic and adiabatic field ionization (see, e.g., Ref. [53]) owing to the lack of angular-momentum degeneracy in nonhydrogenic Rydberg atoms. Whereas for low-lying n_0 values an intense and narrow adiabatic peak is dominating the response function, the diabatic contribution to the ionization signal (occurring at higher field strengths) becomes more and more important with rising principal quantum number. In a transient regime of n_0, most prominently at $n_0=84$ [Fig. 7(b)], the diabatic peak exhibits a clearly developed structure with a larger part at lower [15 V/cm in Fig. 7(b)] field strengths and a broad shoulder at higher fields. This can be seen in Fig. 7, where the normalized response functions $G^{(n_0)}(E)$ are plotted for $n_0=80$, 84, and 88, as well as in Figs. 6(c)–6(g).

The n_0 dependence of the relative importance of adiabatic and diabatic signal contributions, as well as the substructure in the diabatic peak in a certain regime has also been observed in Refs. [51] and [52]. There, the broad diabatic part, extending to relatively high values of the ionizing field, has been assigned to states which hardly mix with other states and ionize predominantly at higher field strength by quantum-mechanical tunneling.

In Figs. 8(a)–8(c), the field-ionization signals $G^{(c)}(E;t)$ of atoms initially prepared in the state $84P_{3/2}$ and afterwards subjected to a coherent microwave field are displayed. The microwave field strength was 1.37 V/cm. The three plots show the response functions $G^{(c)}(E;20$ ns), $G^{(c)}(E;100$ ns), $G^{(c)}(E;1\ \mu$s). All of them have a quite similar shape and are significantly different from $G^{(84)}(E)$, shown in Fig. 7(b). The shoulder structure of the diabatic signal contribution disappears and the ratio between the diabatic and adiabatic peak diminishes, both of these effects reflecting the population change induced by the microwave interaction. It can be seen from Figs. 8(a)–8(c) that the diabatic peak shifts slightly towards higher fields which indicates that the change of the level population goes rather towards smaller than towards higher n values. This is not contradicted by the fact that the ionization signal in Figs. 8(a)–8(c) is not significantly increased on the left wing of the diabatic part. States lying below $84P_{3/2}$ show a less prominent diabatic contribution (see Fig. 6) which does not significantly add to the high field side of the diabatic signal part of $84P_{3/2}$ and is therefore covered by the diabatic contribution [Figs. 8(a)–8(c)]. This conclusion is supported by theoretical calculations (see Sec. IV, Fig. 15).

Contrasting the drastic change of the structure of $G^{(c)}$ [Figs. 8(a)–8(c)] with respect to $G^{(84)}$ [Fig. 7(b)] within less than 20 ns, a comparison of Figs. 8(a)–8(c) gives us a first visual impression of the localization phenomenon which is the topic of this work: The atomic ensemble (initially prepared only in the state $84P_{3/2}$) reaches a practically stationary population distribution after a quite short microwave interaction time.

The delocalization due to noise is demonstrated in Figs. 8(d)–8(f): whereas $G^{(s)}(E;20$ ns) and $G^{(s)}(E;100$ ns) do not yet differ much from $G^{(c)}(E;20$ ns) nor from $G^{(c)}(E;100$ ns), there is a dramatic change in $G^{(s)}(E;1\ \mu$s). The small component of broadband noise with a (externally measured) power R of 12.6 μW—which is $\frac{1}{500}$ of the power of the coherent signal being 6.3 mW—shows its influence only after a relatively long interaction time. It is apparent that the coherent part of the microwave field establishes very fast (within less than 20 ns) a localized population distribution [see Fig. 8(a)] which is then slowly changed by the background noise.

C. Evaluation of the experimental results

In order to quantify the experimental results and for a comparison with the theory as well as with the numerical predictions, we had to extract the time dependence of the Shannon width from the experimentally observed ionization probabilities. This was done by defining

$$W(R,t)=\exp\left[-\sum_{n_0\in J} w(R,t;n_0)\ln w(R,t;n_0)\right], \tag{67}$$

where the vector $\{w(R,t;n_0)|n_0\in J\}$ denotes the solution of the optimization problem

$$\min_{w'}\int |G^{(s)}(E;t)-\sum_{n_0\in J} w'(R,t;n_0)G^{(n_0)}(E)|^2 dE\ ,$$
$$0\le w'(R,t;n_0)\le 1,\ \sum_{n_0} w'(R,t;n_0)=1\ , \tag{68}$$

and where J is a finite set of states $n_0P_{3/2}$, $J=\{64P_{3/2},65P_{3/2},\ldots,129P_{3/2}\}$. The limitation to a set of $P_{3/2}$ states is an approximation which is justified by the fact that the theoretical calculations discussed below (see Fig. 16) show that the average occupation probability of the levels is restricted mainly to states with small angular momentum which show qualitatively the same field-ionization behavior. The $P_{3/2}$ states have the advantage that their ionization behavior can accurately be measured, also for different n_0, after direct population with the laser light.

Before presenting the Shannon width resulting from the deconvolution (68) we should like to make some remarks concerning the comparison of Figs. 6–8 to an actual value of the width as defined in (67). Due to the natural logarithm in (67), small occupation probabilities systematically obtain a larger weight in the calculation of the Shannon width than, e.g., in the calculation of the half width of the population distribution. For distributions with long tails and small probabilities the Shannon width can assume values which are by a factor of 2 to 3

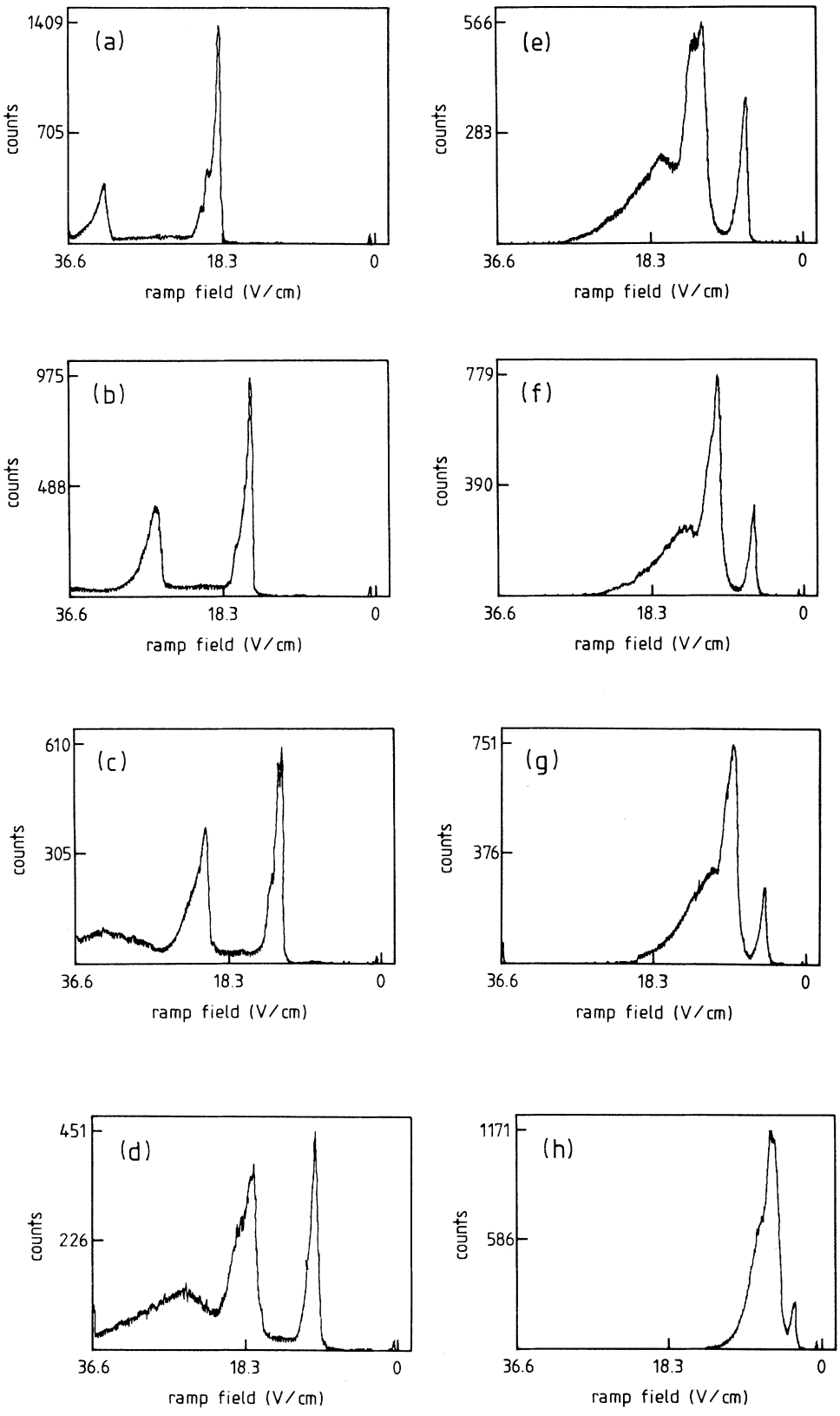

FIG. 6. Non-normalized field-ionization signals $\tilde{G}^{(n_0)}(E)$ of $nP_{3/2}$ states, without microwave interaction. $n_0 =$ (a) 68, (b) 72, (c) 76, (d) 80, (e) 88, (f) 92, (g) 96, and (h) 110.

larger than the corresponding signal half width. In this paper, we use the term "width" to design the value of the Shannon width rather than the half width of the population distribution. Therefore, a drastic spreading of this width of the level distribution may be accompanied by a less significant broadening of, e.g., the half width of the adiabatic peak of the experimentally determined field-ionization signal. This is the case in our experiments, as can be seen from the comparison of Figs. 6–8 to Fig. 9

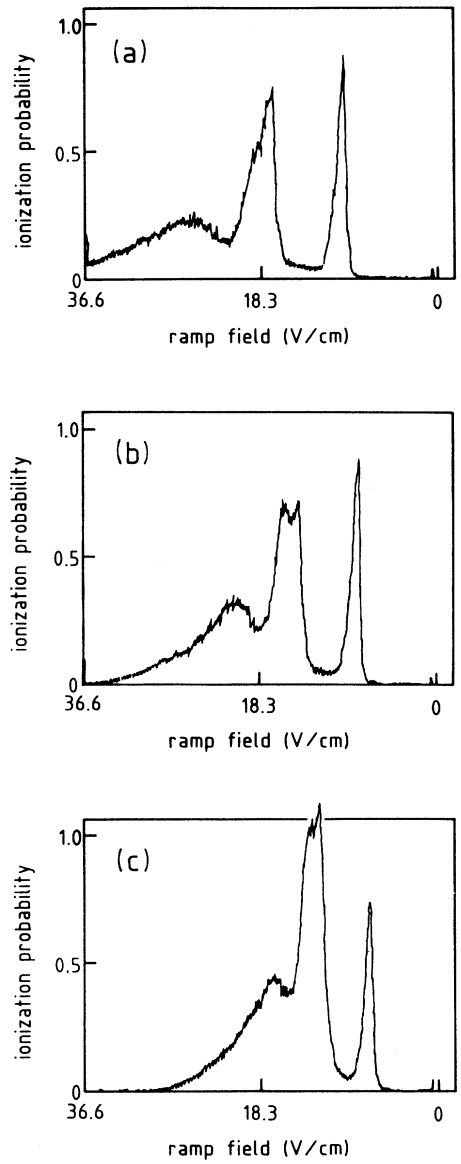

FIG. 7. Normalized field-ionization probabilities $G^{(n_0)}(E)$ without microwave interaction. $G^{(n_0)}(E)$ is obtained from $\tilde{G}^{(n_0)}(E)$ (Fig. 6) by normalization to $\int \tilde{G}^{(n_0)}(E)dE$. The value of this integral was close to 50 000 counts for all the scans displayed in Figs. 6–8. $n_0 =$ (a) 80, (b) 84, (c) 88.

and as will be further discussed and supported by numerical evidence in Sec. IV. Moreover, due to the S, P, and D states, possessing non-negligible and distinct quantum defects δ_l, an adiabatic peak can conceal more energetically distinct levels than in the hydrogenic case since the position of the adiabatic peak in the field-ionization picture obeys the scaling rule $(n_0-\delta_l)^{-4}$. It is this number of energetically distinct levels which is supposed to exhibit the phenomenon of dynamical localization and is approximated by the empirically evaluated width (67) depicted in Fig. 9.

As we can see from Fig. 9, in the presence of only the coherent microwave signal—without noise—the initial spreading of the Shannon width, which leads to an increase from one to a value of somewhere between 12 and 15 within less than 20 ns, is followed by a localized regime where the Shannon width keeps this latter value constant for interaction times very much in excess of 20 ns reaching up to 5 μs. We emphasize that the growth of the width stops despite the fact that there is no obvious barrier in the Rydberg series at a finite value of populated bound states. The "barrier" is dynamical in nature and constitutes the essence of what we are reporting in this paper. The stop of the growth of the width, the "localization," is explained by destructive wave interference which was first discovered by Anderson in the late fifties in the context of localized electron wave functions in disordered solids [54,55]. In the atomic physics context, localization with respect to the energy levels of the Rydberg atoms is revealed by the constancy of the Shannon width in time although the external driving field is continuously acting on the atoms. Localization may be interpreted as the "freezing" of the wave packet [19,49] with respect to the atomic bound states despite continued external perturbation. In terms used by Chirikov, Israelev, and Shepelyansky [5] and Casati, Guarneri, and Shepelyansky [49] this freezing puts an end to the initial spreading behavior which should mimic the classical dynamics, since for interaction times short enough, the atomic system cannot yet resolve the discreteness of the quasienergy spectrum. For a quantitative comparison to Casati's predictions, however, we have to take into account the fact that the level structure of rubidium is much more complicated than the hydrogenic one. It can be assumed that the microwave excitation process of the Rydberg atoms is dominated by one-photon transitions between levels with $l \leq 3$, where we conjecture that the scaled frequency for rubidium atoms should be at least twice as large as in the hydrogenic case. Indeed, recent experimental results [56] support this conjecture. Defining therefore $\omega_0 \approx 2\omega n_0^3$ gives us a value of $\omega_0 \approx 2.18$ for the frequency used in our experiment. For the scaling of the field strength, however, there is no such simple argument. Nevertheless, the coupling of about 14 unperturbed states to the atomic dynamics at a scaled frequency larger than one can be considered as a sufficient condition for the presence of nontrivial dynamical localization. Furthermore, new data [56] confirm that the dynamical localization, which we observe here for the first time, can be interpreted as the quantum-mechanical suppression of classical chaos [37].

Adding noise leads to delocalization at break times t^* which are inversely proportional to the noise power R, as can be seen from Fig. 10. The delocalization occurs at a rate qualitatively independent of R and establishes itself much slower than the initially observed stationary population distribution, which is already established after the first 100 microwave cycles. Both observations are in good agreement with the theoretical predictions [33,34] presented in detail in Sec. II.

IV. DISCUSSION

In this section we discuss the various approximations made in the derivation of the theoretical results presented in Sec. II. We will also have a closer look at the experimental procedure and try to further interpret the experimental results with the help of a time-dependent calculation of the wave function of the rubidium Rydberg electron. In this connection we come back to the remarks about adiabatic switching in the Introduction.

In the theoretical section we made essentially three approximations in the derivation of the master equation: (i) coupling to the heat bath in second-order perturbation theory, (ii) the rotating-wave approximation, and (iii) the Markov approximation. Let us now examine the consistency of these approximations, which are, in fact, closely connected. The Markov approximation requires that the frequency dependence of the response function

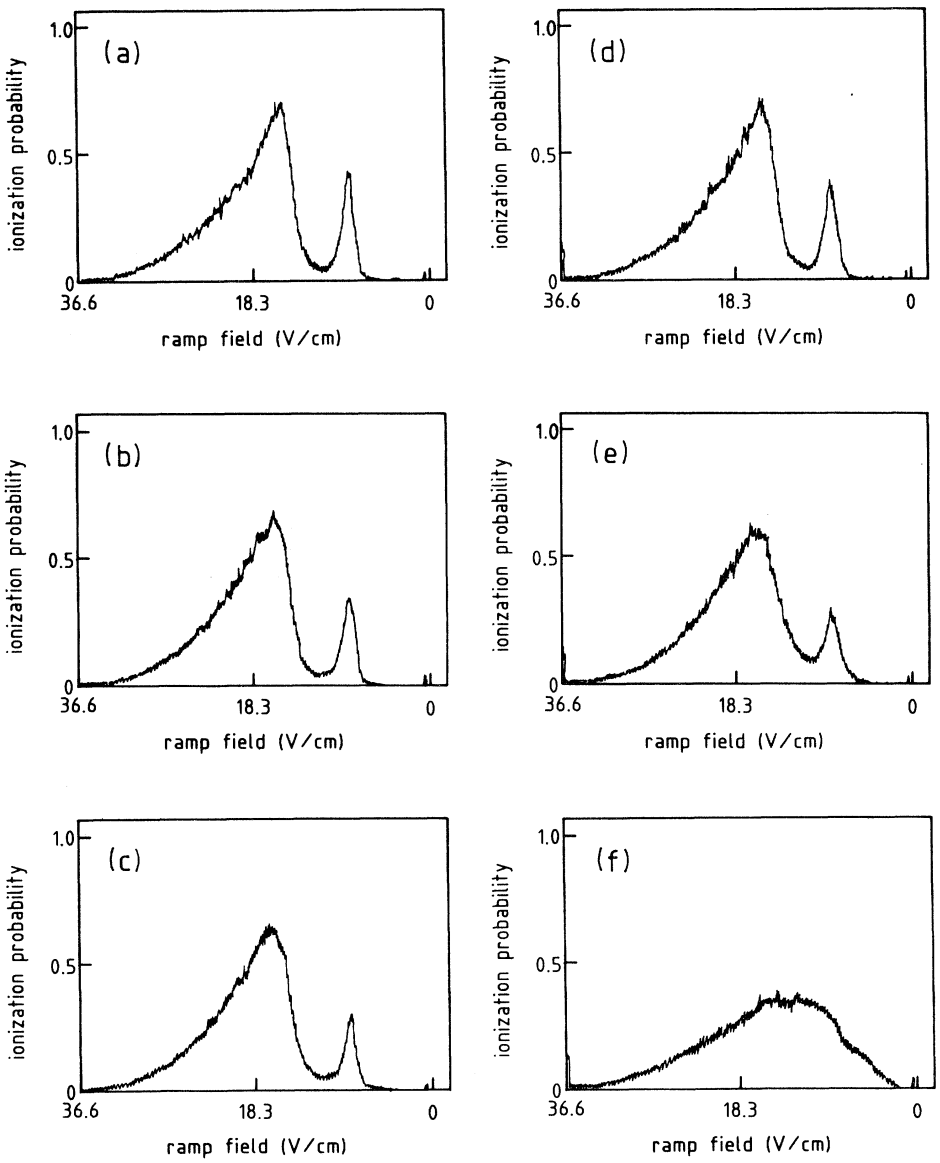

FIG. 8. Field-ionization probabilities for different microwave configurations. (a) $G^{(c)}(E;20\text{ ns})$; power of the coherent signal: 6.3 mW, microwave pulse length: 20 ns. (b) $G^{(c)}(E;100\text{ ns})$; as in (a) but with 100-ns interaction time. (c) $G^{(c)}(E;1\ \mu\text{s})$; as in (a) but with 1-$\mu$s interaction time. (d) $G^{(s)}(E;20\text{ ns})$; as in (a) but with a broadband noise component of total power 12.6 μW. (e) $G^{(s)}(E;100\text{ ns})$; as in (b) but noise power 12.6 μW. (f) $G^{(s)}(E;1\ \mu\text{s})$; as in (c), but noise power 12.6 μW.

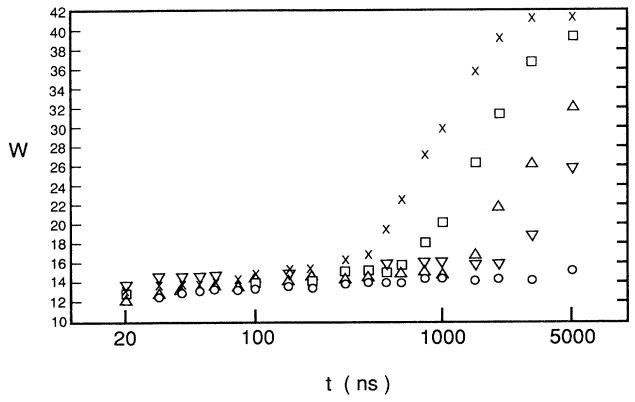

FIG. 9. Time dependence of the Shannon width under the influence of a coherent microwave field (power: 6.3 mW), with different noise contributions: Circles, coherent signal without noise; crosses, additional noise power: 12.6 μW; squares, 6.3 μW; pyramids, 3.2 μW; triangles, 1.6 μW.

$$\chi''(\omega)=2\pi \sum_{m,n,\lambda} \rho_{mn}^{(\lambda)}(\omega)|g_{mn}^{(\lambda)}(\omega)|^2[1+n_{\rm th}(\omega)] \tag{69}$$

be negligible on the frequency scale $\gamma_{\alpha\beta}(k)$, i.e.,

$$\gamma_{\alpha\beta}(k)\frac{d\ln\chi''(\omega)}{d\omega}\bigg|_{\omega=\Omega_{\alpha\beta}(k)} \ll 1 \ . \tag{70}$$

This condition is satisfied if $\Omega_{\alpha\beta}(k)$ is sufficiently different from the cutoff frequencies ω_{mn} where the waveguide (i.e., the reservoir) exhibits resonances, and if $\gamma_{\alpha\beta}(k)\ll\Omega_{\alpha\beta}(k)$. It can be seen both in our numerical results in Fig. 2 and in the experimental results in Figs. 8 and 9 that the rates $\gamma_{\alpha\beta}(k)$ are indeed the smallest rate constants in the system, much smaller than the typical values of the quasienergy spacings, which determine the inverse time scale of the coherent irregular beatings seen in Fig. 2, and also much smaller than the inverse of the characteristic time needed to establish the frozen localized wave packet in Figs. 8 and 9. The Markov approximation, therefore, is well satisfied in the present case. As can be seen from (70) the Markov approximation requires the rate constants to be small on the characteristic frequency scale of the system. The same condition also validates a perturbative calculation of the coefficients of the master equation. Indeed, within the Markov approximation it is even necessary, for the sake of consistency, to limit the accuracy to a second-order treatment, i.e., in a higher-order calculation non-Markovian effects should also appear.

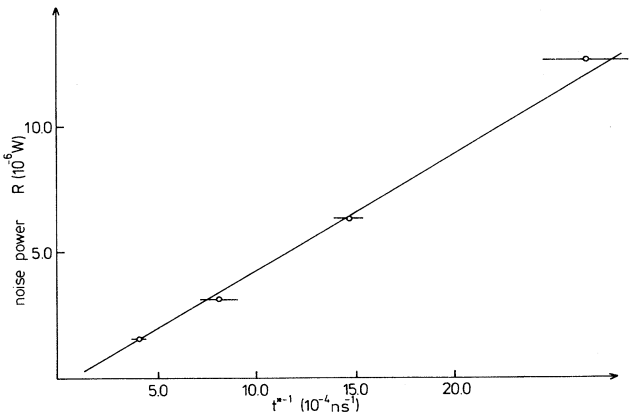

FIG. 10. Relation between noise power and break time t^*, extracted from Fig. 9.

Finally, also the rotating-wave approximation is validated by the fact that the inverse time scale $\gamma_{\alpha\beta}$ is much smaller than $\Omega_{\alpha\beta}$ and therefore the contribution of the rapidly oscillating counterrotating terms are averaged out in a time $\gamma_{\alpha\beta}^{-1}$. Another way of stating this fact is that in the master equation we are only interested in the rates of real transitions, which require energy conservation and therefore come from the terms kept in the rotating-wave approximation, while we are not interested in frequency shifts of the quasienergies, which would also receive (small) contributions from virtual transitions, a part of which is neglected in the rotating-wave approximation.

This finishes the discussion of the three approximations (i)–(iii) mentioned above and we turn our attention to some additional numerical calculations which we performed for the sake of a direct microscopic theoretical understanding and interpretation of the experiments discussed in Sec. III.

We performed a quantum-mechanical calculation of the time evolution of the wave function of a rubidium Rydberg electron launched in the 84P state, simulating the three-dimensional experimental situation. The rubidium atom is subjected to a microwave pulse which was modeled as closely as possible to the experimental conditions. The pulse consists of a burst of microwave power with the electric field given by

$$\begin{aligned} &E_{\rm int}(t)=\varepsilon f(t) \ , \\ &f(t)=f_{\rm on}(t)\sin(\omega t)f_{\rm off}(t) \ , \end{aligned} \tag{71}$$

where the envelope functions $f_{\rm on}$ and $f_{\rm off}$ are chosen to be

$$\begin{aligned} f_{\rm on}(t)&=1-\frac{1}{1+e^{(\omega t-\varphi_i)/d}} , \\ f_{\rm off}(t)&=\frac{1}{1+e^{(\omega t-\varphi_f)/d}} \ , \end{aligned} \tag{72}$$

with $\varphi_i=600$, $\varphi_f=2550$, and $d=100$. This microwave pulse is shown in Fig. 11(a). Figure 11(b) shows the initial stage of the pulse from $N=40$ to 150. According to the experimental situation the pulse climbs in about 70 cycles from 10% to 90% of its strength. Counting the number of cycles in Fig. 11(b) shows that the theoretical pulse fulfills the experimental requirements. The total length of the pulse was chosen to be 500 cycles. The maximal field strength of the pulse (the plateau field) was chosen to be $\xi=1.37$ V/cm. The frequency is 12.059 44 GHz. At the chosen frequency, 500 microwave cycles correspond to a total interaction time of $t_{\rm int}\approx 40$ ns, and

a plateau interaction time of $t_{\text{plat}} \approx 17$ ns. Therefore, the total length of the pulse is on the order of the shortest pulses used in the experiment (compare Fig. 9). It has to be emphasized in this connection that pulses of arbitrary plateau length can always be calculated, once the Schrödinger equation with the pulse (71) is integrated. This stems from the fact that the total time evolution operator over a pulse which is switched on and off can always be written as the product of three propagators,

$$U_{\text{tot}}(\text{pulse}) = U_{\text{off}} U_{\text{plat}}(M) U_{\text{on}} , \tag{73}$$

where it is assumed that the plateau consists of M microwave cycles of constant frequency and amplitude. Therefore, $U(M)$, i.e., the propagator over M cycles, is nothing but the product

$$U_{\text{plat}}(M) = U_{\text{plat}}^{M}(1) \tag{74}$$

of M one-cycle propagators. Clearly, the information contained in the one-cycle propagator $U_{\text{plat}}(1)$ in the plateau region is enough to know $U(M)$ for any arbitrary plateau length M. This is even more evident if (in a finite truncated basis) we spectrally decompose $U(1)$ into its eigenstates [Floquet states, compare (25) for $t = 2\pi/\omega$]

$$U_{\text{plat}}(M) = \sum_{\alpha} |\alpha\rangle e^{i\mu_\alpha M 2\pi/\omega} \langle\alpha| , \tag{75}$$

which is as easily calculated for one cycle as it is for any plateau length M. From (73) it is also evident that the average occupation probabilities of unperturbed atomic states $|n\rangle$ are not dependent on the length M of the plateau and neither is the average localization length. This is easily seen in the following way. Denoting time averages (average over M) by $\langle\ \rangle$, we have in the plateau region:

$$\langle p_{n,n_0} \rangle = \langle |\langle n | U_{\text{plat}}(M) | n_0 \rangle|^2 \rangle = \sum_{\alpha} |\langle n|\alpha\rangle|^2 |\langle \alpha | n_0 \rangle|^2 \tag{76}$$

and this is independent of M if ω is not exactly in resonance with any two quasienergy states $|\alpha\rangle$ and $|\beta\rangle$.

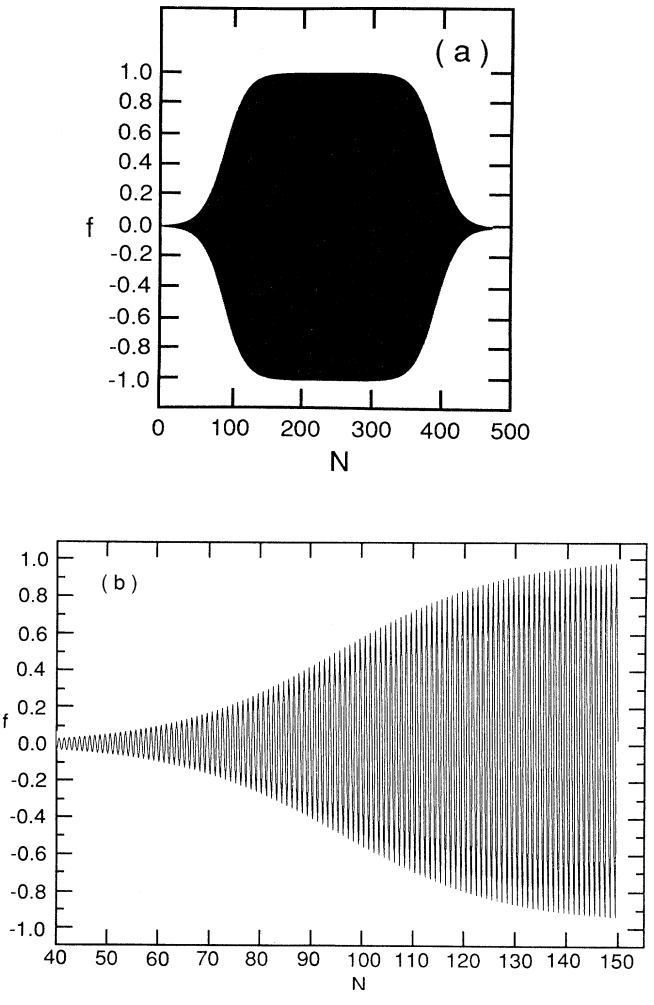

FIG. 11. (a) Microwave pulse profile used in the theoretical calculations of microwave driven rubidium atoms. (b) The rising wing of the pulse on a magnified scale.

The decomposition (73) can also be interpreted more physically. The propagator U_{on} switches the system from the atomic state which was prepared far outside the waveguide (or the cavity), to the beginning of the plateau region. The structure of the propagator U_{plat} governs the time evolution of the atomic system during the plateau stage, where the interaction field is time periodic with a constant amplitude. The role of the switch-on phase is to set up the initial conditions for the propagation with U_{plat}. The structure information contained in U_{plat} is the basis for the understanding of all the processes that happen in the plateau region (like beating between quasienergy states or ionization). As far as the structure of these processes is concerned (e.g., efficient probability transport to ionizing regions of quantum phase space at avoided crossings of quasienergies in the plateau region [41]), they are independent and decoupled from the switch-on stage. On the other hand, the percentage of the participating probability and the initial phases are determined by the switch-on processes.

If bound-space excitations are to be studied by the application of a microwave pulse, special attention has to be paid to the last stage, the switch-off stage, mediated by the propagator U_{off}. If the pulse rises and falls very slowly with respect to internal excitation energy differences (adiabatic situation), U_{off} can act as an efficient "eraser" undoing most of the excitations (in $|nlm\rangle$ space) caused by the application of U_{on} and U_{plat}.

The three different regions, switch on (U_{on}), plateau (U_{plat}), and switch off (U_{off}) were already intensively studied in Refs. [25] and [57]. The point of presenting our results on microwave-driven rubidium atoms is therefore not to elaborate on existing theory but rather to model the experiment as closely as possible in order to provide further insight into the dynamics of our particular experimental situation. In particular we will see that our experiments are conducted in an adiabatic regime as far as microwave switching is concerned [57,58].

The basis functions chosen for the calculations are

$\{|nlm\rangle\}n=78,\ldots,100$ (principal quantum number), $l=0,\ldots,8$ (angular momentum), and $m=0$ (magnetic quantum number). The spin of the electron, and therefore the rubidium fine structure, are neglected. Quantum defects in the single-particle energies, on the other hand, are included in the calculations. We chose [59,60] $\delta_0=3.13$, $\delta_1=2.64$, $\delta_2=1.35$, $\delta_{l>2}=0$ for the quantum defects. The wave function is expanded according to

$$|\Psi(t)\rangle=\sum_{n,l} A_{nl}(t)|nlm=0\rangle \tag{77}$$

and we denote by

$$P_{nl}(N)=\left|A_{nl}\left[N\frac{2\pi}{\omega}\right]\right|^2$$

the probability distribution of the wave packet over principal and angular-momentum quantum numbers after N cycles of the microwave field.

Figure 12(a) shows the probability distribution $P_{nl}(60)$ of a rubidium wave function started in the state $|n=84, l=1, m=0\rangle$ after 60 microwave cycles. The wave function is sharply peaked at the position of the starting state since the field had just about reached its 10% value and the packet hardly had any time to spread. In Fig. 12(b) we show $P_{nl}(250)$, i.e., the probability distribution for a time which corresponds to the middle of the pulse plateau. The wave packet is now considerably broader and extends from $n=80$ to 86, and from $l=0$ to 5. Figure 13 shows a logarithmic plot of the probability distribution of Fig. 12(b). It is seen that on a logarithmic scale (the proper scale for the investigation of localization phenomena) the probability distribution is very broad. Figure 12(c) shows the wave packet after 440 cycles of the microwave field, i.e., at a time when the pulse is nearly switched off again. It is clearly seen that practically all the excitation probability, in fact 98.27%, has come back to the starting state. After 500 cycles the starting state is occupied with 99.98% of the probability.

Clearly the excitation process displayed by our model rubidium atom is very adiabatic [57] and one may wonder whether the basis chosen for the representation of our results in Figs. 12–16 is the most convenient basis. On the other hand, the phenomenon of localization in the sense used in this paper, and especially the concept of a localization length [5], is strongly basis dependent. Since the experiment detects occupation probability in the eigenstates of the unperturbed atom, we are interested in localization in the $|nlm\rangle$ basis, and this is why we chose to represent our results in this particular basis.

An additional calculation with a faster pulse (11 cycles rise time from 10% field strength to 90% field strength, total pulse length 120 cycles) yielded qualitatively the same results. Due to the faster rise time, however, this pulse leaves the states $|n=84, l=1\rangle$ (88.77%), $|n=88,l=5\rangle$ (1.03%), $|n=88,l=7\rangle$ (4.58%), $|n=92, l=4\rangle$ (2.00%), $|n=95,l=4\rangle$ (1.46%) appreciably ($P_{nl}>1\%$) occupied.

Taken at face value, the theoretical calculations indicate that with the pulses presently used in the experiment, the largest spreading of the wave packet, which occurs during the pulse plateau, is not accessible to experimental analysis. For a final conclusion, however, the theoretical calculations have to take the coupling to the continuum and residual noise into account. It is possible that "noise" is also simulated by avoided crossings which

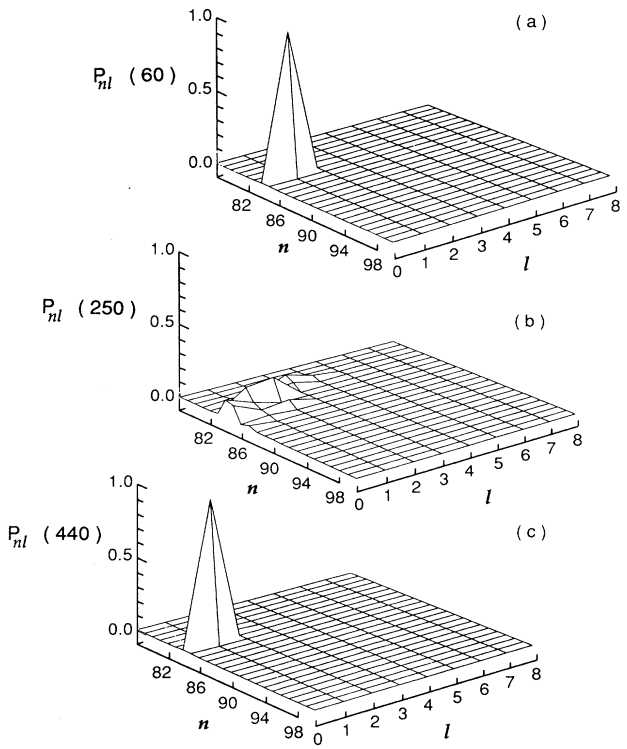

FIG. 12. Calculated probability distribution of a wave packet launched in the 84P state of rubidium and irradiated with the pulse whose profile is shown in Fig. 11. The probability distribution of the wave packet over principal quantum numbers n and angular momenta l is shown after (a) 60, (b) 250, and (c) 440 cycles of the microwave field.

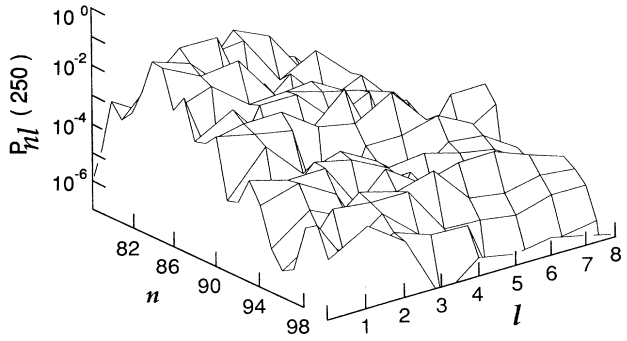

FIG. 13. Same as Fig. 12(b) but on a logarithmic scale relevant for the investigation of localization properties. The wave packet is seen to be very broad in this representation.

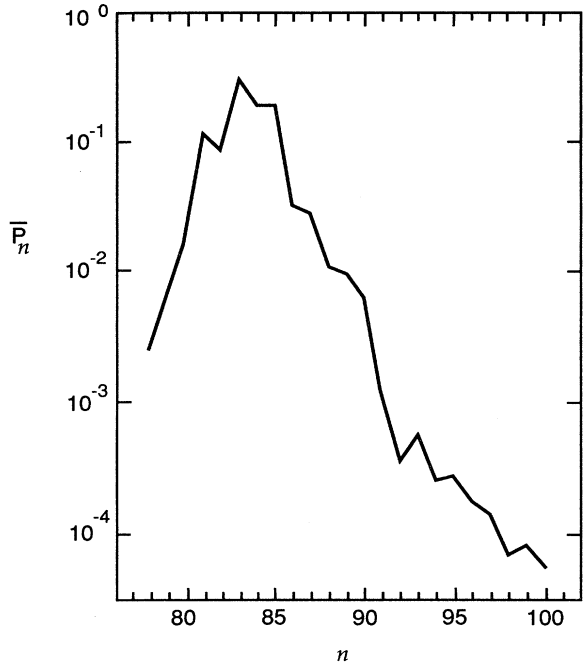

FIG. 14. Average occupation probability $\bar{P}_n$ as a function of the principal quantum number n averaged over 101 microwave cycles from cycle number 200 to 300 in the plateau region of the pulse shown in Fig. 11.

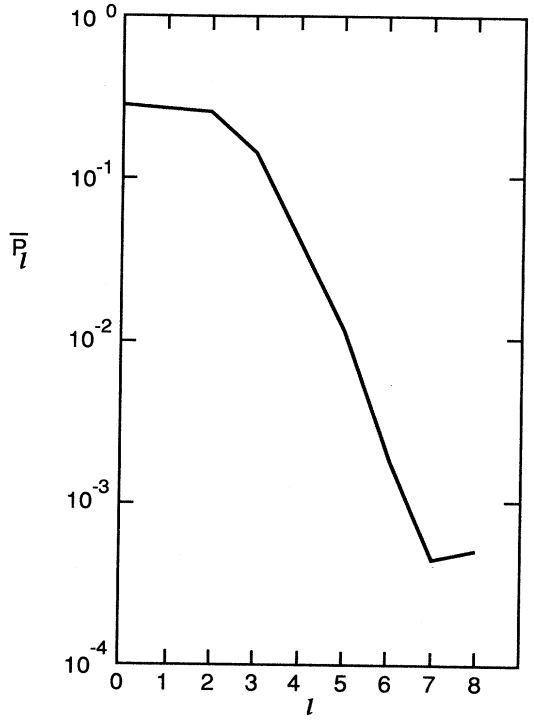

FIG. 16. Average occupation probability $\bar{P}_l$ as a function of the angular-momentum quantum number l averaged as described in Fig. 14.

are due to the fine structure. All these processes, if sufficiently weak, may change phase relations in the bounded space without inducing transitions. Given sufficient time for noise and continuum to act, the phases will not be right at the beginning of the switch-off stage of the pulse and the occupation probability is less likely to return to the starting state. This point was confirmed by the results of some additional calculations which were done within the framework of the one-dimensional hydrogen model. It turns out that the relation between the final-state probability distribution (after the pulse is over) and the localized probability distribution in the pulse plateau region is a complicated function of noise power, continuum coupling strength, pulse shape, and pulse duration. We plan to address this difficult issue in a separate publication. However, assuming that the mechanisms described above destroy at least partly the adiabaticity of the investigated process, there is quite a good agreement between the experimental and numerical results: Calculating the Shannon width of the population distribution along the pulse plateau according to

$$W=\exp\left[-\sum_{n,l} P(n,l)\ln P(n,l)\right], \tag{78}$$

we obtain for the total width $W=18.0$ bound states, which is in qualitative agreement with the results plotted in Fig. 9. Furthermore, we can use the reduced probabilities $P_n(N)=\sum_l P_{nl}(N)$ and $P_l(N)=\sum_n P_{nl}(N)$, to calculate the width of the distribution in n and l, since $P_n(N)$ and $P_l(N)$ give the occupation probabilities of an n state (trace over l) and an angular-momentum state l (trace over n), respectively, $P_n(N)$ and $P_l(N)$ characterize the localization in n and l directions. Figure 14 shows $\bar{P}_n=\frac{1}{101}\sum_{q=200}^{300} P_n(q)$, the average n occupation probability, and Fig. 16 shows $\bar{P}_l=\frac{1}{101}\sum_{q=200}^{300} P_l(q)$, the average l occupation probability, both averaged over 101 cycles in the plateau region of the pulse, on a log scale. It is seen that for the experimental field parameters the wave packet is indeed approximately exponentially localized in both n and l directions. The localization in l is consistent with a dominance of S-P-D(-F) transitions as conjectured in

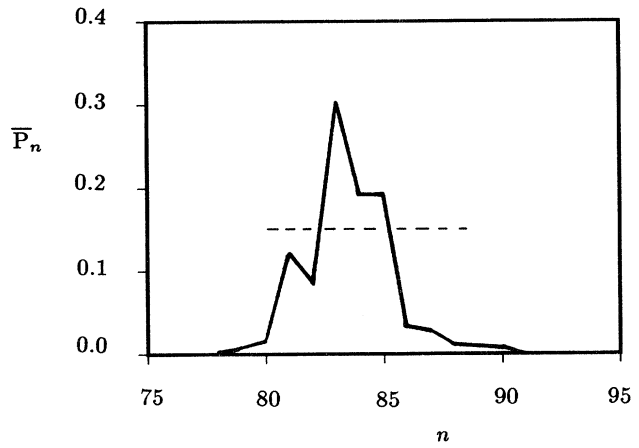

FIG. 15. Same as Fig. 14 but on a linear scale. The dashed line indicates the half width of the distribution.

Sec. II C and in Refs. [35] and [56].

The width in l is obtained to be 4.6 states. The width in n is 6.9 states, being more than twice as large as the half width of $\bar{P}_n$ which is equal to 3, as can be seen from Fig. 15 where $\bar{P}_n$ is plotted on a linear scale. This supports the discussion on the numerical difference between the concepts of "Shannon width" and the "half width" presented in Secs. II C and III C of this paper.

Experimental knowledge of the detailed (n,l) state probability distribution in the plateau region of the pulse is clearly desirable, since it provides the necessary information for extracting the localization length of the wave packet from the experimental data. On the other hand, the probability distribution after the pulse is switched off is far more easily accessible with the current setup and provides valuable information on the phase coherence of the wave function during the microwave irradiation stage. The destruction of phase coherence by the applied (technical) noise is measured by the degree of spreading of the wave packet after the microwave pulse is switched off, i.e., by the degree of deviation from the nontrivially localized population distribution which is induced by the coherent component of the field. A large deviation of the packet from this latter level distribution, the width of which is already significantly larger than the one of the starting state, indicates the influence of noise. From the change in the width, therefore, one can indeed uniquely extract the N^* transition points and compare to the theoretical predictions. Concluding this section we can say that the experiment described in Sec. III is indeed appropriate for the investigation of the localization behavior of wave packets in strong radiation fields and of the influence of noise on wave-packet dynamics.

V. SUMMARY AND CONCLUSIONS

To summarize, we derived and solved a master equation for Rydberg atoms in strong noisy microwave fields which is based on the atomic Floquet states rather than the unperturbed atomic states. Based on this theoretical approach we predicted the existence of four regimes in the dynamics of Rydberg atoms strongly driven by noisy microwave fields. We established the existence of a critical interaction time which marks the end of localization and the beginning of noise-induced diffusion. The scaling behavior of this critical interaction time with temperature (or noise power) was derived. All the theoretical predictions were verified by an experiment with rubidium atoms which was also presented in detail in this paper. We also reported on the first explicit experimental observation of nontrivial dynamical localization of Rydberg atoms in a strong coherent monochromatic microwave field, the localization being manifest in the "freezing" of the quantum-mechanical wave packet. The addition of a perturbative noise component to the coherent signal—in extension of a first experimental evidence published earlier [33]—was shown to lead to delocalization on a time scale which agrees with theoretical predictions as well as with numerical simulations.

ACKNOWLEDGMENTS

We thank H. P. Breuer, K. Dietz, and M. Holthaus for discussions and useful suggestions. One of us (R.G.) would like to thank the Deutsche Forschungsgemeinschaft for support via the "Sonderforschungsbereich 237, Unordnung and grosse Fluktuationen." U.S. and H.W. acknowledge financial support by Stiftung Volkswagenwerk. R.B. is grateful for support by the NSF under Grant No. CHE88-19436 and for support by the Deutsche Forschungsgemeinschaft.

---

*Present address: Department of Physics, University of Delaware, Newark, DE 19716.

†Present address: Laboratoire de Spectroscopie Hertzienne de l'Ecole Normale Supérieure, Université Pierre et Marie Curie, 4 Place Jussieu, T12-E01, 75252 Paris CEDEX 05, France.

‡Permanent address: Department of Physics, Polish Academy of Sciences, aleja Lotników 32/46, 02-668 Warszawa, Poland. Present address: Department of Physics, State University of New York at Stony Brook, Stony Brook, NY 11794-3800.

§Permanent address: Department of Nuclear Physics, The Weizmann Institute of Science, 76100 Rehovot, Israel.

[1] A. J. Lichtenberg and M. A. Lieberman, *Regular and Stochastic Motion* (Springer, Berlin, 1983).

[2] G. Casati, B. V. Chirikov, D. L. Shepelyansky, and I. Guarneri, Phys. Rep. **154**, 77 (1987).

[3] R. Blümel and U. Smilansky, Phys. Rev. Lett. **58**, 2531 (1987).

[4] R. Blümel and U. Smilansky, Z. Phys. D **6**, 83 (1987).

[5] B. V. Chirikov, I. M. Izraelev, and D. L. Shepelyansky, Sov. Sci. Rev. Sec. C **2**, 209 (1981).

[6] T. F. Gallagher and W. E. Cooke, Phys. Rev. Lett. **42**, 835 (1979).

[7] W. P. Spencer, A. G. Vaidyanathan, D. Kleppner, and T. W. Ducas, Phys. Rev. A **25**, 380 (1982).

[8] E. Ott, T. M. Antonsen, Jr., and J. D. Hanson, Phys. Rev. Lett. **53**, 2187 (1984).

[9] S. Adachi, M. Toda, and K. Ikeda, Phys. Rev. Lett. **61**, 655 (1988).

[10] B. Meerson, Phys. Rev. Lett. **62**, 1615 (1989).

[11] D. Cohen, Phys. Rev. A **43**, 639 (1991).

[12] H. Ritsch and P. Zoller, Phys. Rev. Lett. **61**, 1097 (1988).

[13] K. Arnett, S. J. Smith, R. E. Ryan, T. Bergeman, H. Metcalf, M. W. Hamilton, and J. R. Brandenberger, Phys. Rev. A **41**, 2580 (1990).

[14] C. W. Gardiner, Phys. Rev. Lett. **56**, 1917 (1986).
[15] C. W. Gardiner and M. J. Collett, Phys. Rev. A **31**, 3761 (1985).
[16] G. P. Agrawal, Phys. Rev. A **37**, 2488 (1988).
[17] G. Gray and R. Roy, Phys. Rev. A **40**, 2452 (1989).
[18] A. O. Caldeira and A. J. Leggett, Ann. Phys. (N.Y.) **140**, 374 (1983).
[19] J. E. Bayfield and D. W. Sokol, Phys. Rev. Lett. **61**, 2007 (1988).
[20] J. E. Bayfield and D. W. Sokol, in *Physics of Atoms and Molecules,* edited by K. T. Taylor, M. H. Nayfeh, and C. W. Clark (Plenum, New York, 1988).
[21] E. J. Galvez, B. E. Sauer, L. Moorman, P. M. Koch, and D. Richards, Phys. Rev. Lett. **61**, 2011 (1988).
[22] L. Moorman, E. J. Galvez, B. E. Sauer, A. Mortazawi-M., K.A.H. van Leeuwen, G. v. Oppen, and P. M. Koch, Phys. Rev. Lett. **61**, 771 (1988).
[23] J. E. Bayfield, G. Casati, I. Guarneri, and D. W. Sokol, Phys. Rev. Lett. **63**, 364 (1989).
[24] H. P. Breuer, K. Dietz, and M. Holthaus (unpublished).
[25] H. P. Breuer and M. Holthaus (unpublished).
[26] E. V. Shuryak, Zh. Eksp. Teor. Fiz. **71**, 2039 (1976).
[27] D. R. Grempel, R. E. Prange, and S. Fishman, Phys. Rev. A **29**, 1639 (1984).
[28] T. Dittrich and R. Graham, Europhys. Lett. **7**, 287 (1988).
[29] H. Haken, *Encyclopedia of Physics,* edited by S. Flügge (Springer, Berlin, 1970), Vol. XXV/2c.
[30] W. H. Louisell, *Quantum Statistical Properties of Radiation* (Wiley, London, 1973).
[31] W. Heitler, *Quantum Theory of Radiation* (Clarendon, Oxford, 1954).
[32] R. Blümel, J. Goldberg, and U. Smilansky, Z. Phys. D **9**, 95 (1988).
[33] R. Blümel, R. Graham, L. Sirko, U. Smilansky, H. Walther, and K. Yamada, Phys. Rev. Lett. **62**, 341 (1989).
[34] R. Blümel, R. Graham, L. Sirko, U. Smilansky, H. Walther, and K. Yamada, in *Fundamentals of Laser Interactions II,* edited by Fritz Ehlotzky, Lecture Notes in Physics Vol. 339 (Springer-Verlag, Berlin, 1989).
[35] A. Buchleitner, L. Sirko, and H. Walther, in *Proceedings of the Adriatico Research Conference Quantum Chaos, Trieste, 1990,* edited by H. Ceroleira and R. Ramaswamy (World Scientific, Hong Kong, 1991).
[36] C. E. Shannon, Bell. Syst. Technol. J. **27**, 379 (1948); **27**, 623 (1948).
[37] R. Blümel and U. Smilansky, Phys. Rev. Lett. **52**, 137 (1984).
[38] R. Blümel and U. Smilansky, Phys. Rev. A **30**, 1040 (1984).
[39] R. V. Jensen, Phys. Rev. A **30**, 386 (1984).
[40] D. L. Shepelyansky, in *Chaotic Behavior in Quantum Systems,* edited by G. Casati (Plenum, New York, 1985), p. 187.
[41] R. Blümel and U. Smilansky, J. Opt. Soc. Am. B **7**, 664 (1990).
[42] G. Casati, B. V. Chirikov, F. M. Izraelev, and J. Ford, in *Stochastic Behavior in Classical and Quantum Hamiltonian Systems,* edited by G. Casati and J. Ford, Lecture Notes in Physics Vol. 93 (Springer, Berlin, 1979), p. 334.
[43] T. Dittrich and R. Graham, Z. Phys. B **62**, 515 (1986).
[44] T. Dittrich and R. Graham, Ann. Phys. (N.Y.) **200**, 363 (1990).
[45] J. A. Gallas, G. Leuchs, H. Walther, and H. Figger, in *Advances in Atomic and Molecular Physics,* edited by D. R. Bates and L. Esterman (Academic, New York, 1985), Vol. 20, p. 413, and references therein.
[46] See, for comparison, T. R. Gentile, B. J. Hughey, D. Kleppner, and T. W. Ducas, Phys. Rev. A **40**, 5103 (1989).
[47] L. Sirko, A. Buchleitner, and H. Walther, Opt. Commun. (to be published).
[48] B. Oumarou, J. Picart, N. Tran Minh, and J. Chapelle, Phys. Rev. A **37**, 1885 (1988).
[49] G. Casati, I. Guarneri, and D. L. Shepelyansky, IEEE J. Quantum Electron. **24**, 1420 (1988).
[50] A. Buchleitner, thesis, Ludwig-Maximilians-Universität München, 1989 (unpublished).
[51] J.H.M. Neijzen and A. Dönszelmann, J. Phys. B **15**, L87 (1982).
[52] J.H.M. Neijzen and A. Dönszelmann, J. Phys. B **15**, 1981 (1982).
[53] T. H. Jeys, G. W. Foltz, K. A. Smith, E. J. Beiting, F. G. Kellert, F. B. Dunning, and R. F. Stebbings, Phys. Rev. Lett. **44**, 390 (1980).
[54] P. W. Anderson, Phys. Rev. **109**, 1492 (1958).
[55] For a recent review on localization see Phys. Today **44** (5), 32 (1991).
[56] M. Arndt, A. Buchleitner, R. Mantegna, and H. Walther (unpublished).
[57] H. P. Breuer and M. Holthaus, Z. Phys. D **11**, 1 (1989).
[58] H. P. Breuer, K. Dietz, and M. Holthaus, Z. Phys. D **10**, 13 (1988).
[59] J. Lorenzen and K. Niemax, Phys. Scr. **27**, 300 (1983).
[60] D. Meschede, J. Opt. Soc. Am. B **4**, 413 (1987).